Chapter One

1.1 Introduction :

More than 600,000 people die from hepatocellular carcinoma (HCC) each year. Worldwide research on the disease needs to be intensified in both the medical and pharmaceutical fields, especially with a focus on providing help to areas where resources are limited. Treatment approaches depend on the stage of the disease at diagnosis and on access to complex treatment regimens. However, advanced disease is not curable, and management of advanced disease is expensive and only marginally effective in increasing quality-adjusted life-years. The delivery of health-care services for HCC can be improved by developing centers of excellence. Concentrating medical care in this way can lead to an increased level of expertise, so that resections are performed by surgeons who understand liver disease and the limitations of resection and other relevant procedures "World Gastroenterology Organization, 2009".

HCC is the sixth most common malignancy worldwide. It is the fifth most common malignant disease in men and the eighth most common in women. It is the third most common cause of death from cancer, after lung and stomach cancer. HCC is the most common malignant disease in several regions of Africa and Asia (Y. Hoshida, A etal, 2008).

Other important factors include poor compliance, with inadequate or absent attendance in surveillance programs and thus late presentation of patients with large tumors; low awareness of the benefits of HCC treatment and ways of preventing underlying liver disease; and a negative opinion among some physicians about screening." World Gastroenterology Organization, 2009.

HCC is associated with liver disease independently of the specific cause of the disease either; infectious: chronic hepatitis B or C., nutritional and toxic: alcohol, obesity (nonalcoholic

fatty liver disease), aflatoxin (co-factor with HBV), tobacco. Secondly, genetic: tyrosinosis, hemochromatosis (iron overload). However, iron overload as a cause per se and as a result of dietary intake (due to cooking in iron pots) is a subject of controversy. α1-Antitrypsin deficiency. Immunologic: autoimmune chronic active hepatitis, primary biliary cirrhosis " World Gastroenterology Organization, 2009".

Computed Tomography (CT) in now a widely applied tool for diagnosis of hepatic tumors. The visual analysis of image series, acquired usually before a contrast product injection and during its propagation, enables doctors to detect lesions and to recognize, to a certain extent, the type of pathology. However, in most cases, visual inspection of CT scans could not be sufficient for proper image interpretation. Even for experienced radiologists, the correct differentiation of tumor affected tissue is a difficult task. The definitive diagnosis often requires invasive procedures like needle biopsy or even surgery, which carry a risk of complications. New computer-aided image processing methods (in particular methods of their texture analysis), in combination with effective classification algorithms, can considerably improve the accuracy of the diagnosis. Extracting the information not normally detected by the human eye, those techniques could reduce or even eliminate the necessity of performing the invasive techniques (Bruno A., et al 1997)

An objective and explicit characterization of image regions is one of the crucial problems to deal with when a computer aided image analysis is performed. One of the most useful sources of information about analyzed image regions could be their texture [Haralick R. M]. The texture analysis consists in extracting a set of numerical parameters (so-called texture features) to characterize Regions of Interest (ROIs) defined in the organs under study. Each of the texture parameters expresses a specified property of the texture, like coarseness, homogeneity, or the local contrast. So far, a great variety of texture features extraction methods has been investigated. [Galloway M. M et al 1998].

The first application of texture analysis for characterization of pathologically changed regions of liver tissue in tomographic images was presented in [Mir A. H., et al 1995]. In the work it was shown that values of the gray level distribution derived from the run- length matrix were significantly different in normal and malignant tissue. [Chen ,et al 1989] proposed an automatic diagnostic system for CT liver image classification that was able to automatically find, extract the liver boundary and to further classify its two major malignant lesions. The system used an artificial neural network in combination with fractal and co-occurrence features. A similar approach (the back- propagation neural network based on first order and co-occurrence features) was applied to recognizing a normal and abnormal liver [Husain , et al 2000]. In the combination of four different fractal dimension estimators (corresponding to the power spectrum method, box counting method, the morphological fractal estimator and the kth-near- est neighbor method) and the fuzzy C-Means algorithm were applied to differentiate normal liver parenchyma from hepatocellular carcinoma. Recently presented a system that used co-occurrence descriptors and three sequentially placed feed-forward neural networks for classification of normal and pathological liver regions. Finally, in a computer-aided diagnostic system to classify focal liver lesions by an ensemble of neural network and statistical classifiers was proposed. This system used first order statistics, co-occurrence matrix and gray-level difference matrix features, Laws' texture energy measures, and fractal dimension estimators to characterize four different types of liver tissue. All aforementioned systems were applied to non-enhanced CT scans and did not consider dynamic CT. In our investigations , texture classification of the hepatic metastasis was performed on the basis of dynamic CT. Images corresponding to three acquisition phases (non-enhanced images and after a contrast product injection, in arterial and portal phases) were analyzed separately. It was shown that considering the acquisition moments could improve the classification accuracy. In [Duda D., et al 2004], for the first time, three CT scans with the same slice position and corresponding to

three acquisition moments were analyzed simultaneously. The preliminary results showed that taking into account texture evolution when the contrast product is propagated led to a considerably better image recognition[Duda D., et al 2004].

Only cancers that start in the liver are called liver cancer. To understand liver cancer, it helps to know about the normal structure and function of the liver. The liver is the largest internal organ. It lies under your right ribs just beneath your right lung. It is shaped like a pyramid and divided into right and left lobes. The lobes are further divided into segments (American Cancer Society. Cancer Facts & Figures 2014) .

Unlike most other organs, the liver gets blood from 2 sources: the *hepatic artery* supplies the liver with blood rich in oxygen from the heart, and the *portal vein* brings nutrient-rich blood from the intestines (American Joint Committee on Cancer 2010).

You cannot live without your liver. It has several important functions:

- It breaks down and stores many of the nutrients absorbed from the intestine that your body needs to function. Some nutrients must be changed (metabolized) in the liver before they can be used by the rest of the body for energy or to build and repair body tissues.
- It makes most of the clotting factors that keep the body from bleeding too much when you are cut or injured.
- It secretes bile into the intestines to help absorb nutrients (especially fats).
- It filters out and breaks down toxic wastes in the blood, which are then removed from the body.

1.2 Problem of study:

Generally in radiology the pathology or any abnormality was diagnosed by the radiologist as abnormal area if it reveals agreed upon defect on the image. This trend of diagnosis depend on visual perception; which is subjective and affected by many factors like experiences, oversight and so on. This situation leads sometimes to send normal patient to biopsy as well as abnormal patient might not been send to biopsy for conformation . Therefore texture analysis can provide second opinion for the radiologist to diagnose liver pathology with some confident as well as it will draw his attention to the area of interest.

1.3 Objectives:

1.3.1 General Objectives: is to characterize Hepatocellular carcinoma in CT abdominal images using higher order statistic and Daubechies wavelet coefficient in order to reduce the miss detection rate as well as, to limit the usage of biopsy.

1.3.2 Specific objective:

- To write an algorithm and function that can be used to extract textural feature from CT images
- To extract texture feature from liver tissue and HCC tissue (ROI).
- To extract texture feature using Linear discriminant analysis.
- To delineate the ROI (HCC) on the CT images.
- To classify the extracted features using Grey Level Run Length Matrix (GLRLM).
- To classify the extracted features using Daubechies wavelet.
- To calculate the sensitivity, specificity and accuracy.

1.4 Overview of study:

This study is concerned with characterization of hepatocellular carcinoma in CT image using higher order statistic and Daubechies coefficient, it falls into five chapters. Chapter one is an introduction, which include preparation of the problem of study and hepatocellular carcinoma, and liver as vital organ in human body as well as statement of the problem and study objectives. While Chapter two will include a comprehensive scholarly literature reviews concerning the previous studies. Chapter three deals with the methodology, where it provides an outline of material and methods used to acquire the data in this study as well as the method of analysis approach. While the results were presented in chapter four, and finally Chapter five include discussion of results, conclusion and recommendation followed by references and appendices.

Chapter two

Literature review

2.1 Hepatocellular Carcinoma:

HCC its Most primary liver cancers are classified as hepatocellular carcinoma. Hepatocellular carcinoma is a malignant tumor composed of cells resembling hepatocytes ; however, the resemblance varies with the degree of differentiation . Hepatocellular carcinoma is commonly associated with cirrhosis (Figure 2.1)

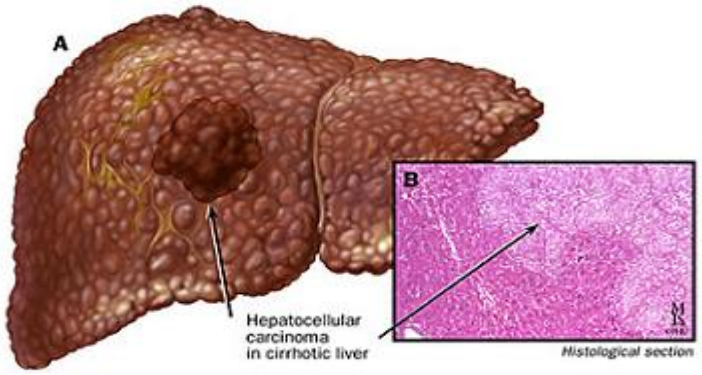

Figure 2.1. A, Cirrhotic liver with focal tumor; B, histological appearance

This type of liver cancer is potentially curable by surgical resection. However, only those patients with localized disease are surgical candidates. Liver function impairment and degree of tumor localization determine patient prognosis proliferation . Clinical trials offer alternative treatment options for patients who are not candidates for resection (Ahmet Gurakar et al 2013).

2.1.1 Symptoms of HCC:

In the U.S., a significant number of hepatocellular carcinoma cases are detected during surveillance or investigation of underlying liver disease. Often, patients present with symptoms related to their underlying liver disease. In a report from Hong Kong, 76% of patients with

hepatocellular carcinoma presented to their hepatoma clinic with abdominal distention or discomfort; less common presentations included weight loss (4.4%), gastrointestinal hemorrhage (4.4%), and jaundice (2.6%). In the Hong Kong series, only 2% were asymptomatic. Rarely, hepatocellular carcinoma can present as an acute abdomen resulting from spontaneous rupture of the tumor into the peritoneal cavity. Hepatocellular carcinoma should be considered in the differential diagnosis of hemorrhagic ascites (Ahmet Gurakar et al 2013).

2.1.2 Anatomy of liver:

The liver is the largest organ in the abdominal cavity and the most complex. It consists of a myriad of individual microscopic functional units call lobules. The liver performs a variety of functions including the removal of endogenous and exogenous materials from the blood, complex metabolic processes including bile production, carbohydrate homeostasis , lipid metabolism, urea formation, and immune functions.

The liver arises from the ventral mesogastrium and only the upper posterior surface is outside of thatstructure. The ligamentum teres and falciform ligament connect the liver to the anterior body wall. The lesser omentum connects it to the stomach and the coronary and triangular ligaments to the diaphragm. The liver is smooth and featureless on the diaphragmatic surface and presents with a series of indentations on the visceral surface where it meets the right kidney, adrenal gland, inferior vena cava, hepatoduodenal ligament and stomach (Figure 2), (Ahmet Gurakar et al 2013)

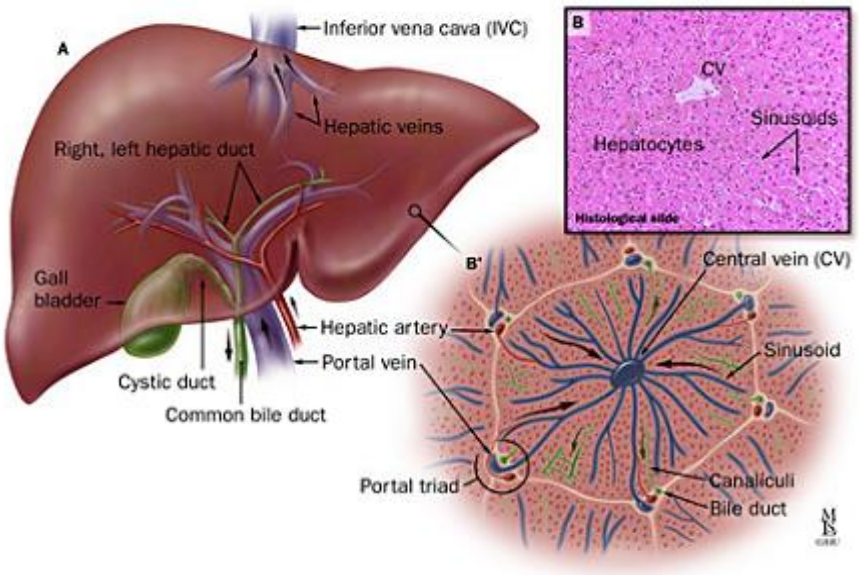

Figure 2.2 .A, Normal gross anatomy of a liver; B, histological slide; B', histological view.

The liver can be considered in terms of blood supply hepatocytes, Kuepfer cells and biliary passages. The liver receives its blood supply from the portal vein and hepatic artery, the former providing about 75% of the total 1500 ml/min flow. Small branches from each vessel the terminal portal venule and the terminal hepatic arteriole enter each acinus at the portal triad. Pooled blood then flows through sinusoids between plates and hepatocytes in order to exchange nutrients. The hepatic vein carries efferent blood into the inferior vena cava and a supply of lymphatic vessels drains the liver (Ahmet Gurakar et al 2013).

Parenchymal cells or hepatocytes comprise the bulk of the organ and carry out complex metabolic processes. Hepatocytes are responsible for the liver's central role in metabolism (Figure 2.2 B'). These cells are responsible for the formation and excretion of bile ; regulation of cabohydate homeostasis ; lipid synthesis and secretion of plasma lipoproteins; control of cholesterol metabolism; and formation of urea, serum albumin, clotting factors, enzymes, and numerous proteins. The liver also aids in the metabolism and detoxification of drugs and other foreign substances.

Kupffer cells line the hepatic sinusoids and are part of the reticuloendothelial system, filtering outminute foreign particles, bacteria, and gut-derived toxins. They also play a role in immune processes that involve the liver. Biliary passages begin as tiny bile canaliculi formed by hepatocytes. These microvilli -lined structures progress into ductules, interlobular bile ducts, and larger hepatic ducts. Outside the porta hepatis, the main hepatic duct joins the cystic duct from the gallbladder to form the common bile duct, which drains into the duodenum (Ahmet Gurakar et al 2013).

2.1.3 Causes of HCC :

Hepatitis B and C : The two most important etiological factors contributing to hepatocelluar carcinoma are hepatitis B andhepatitis C (Figure 2.3). In parts of China and Taiwan, 80% of hepatocellular carcinoma is due to hepatitis B. In the United States and Europe, hepatitis C and hepatitis B contribute equally to disease cases. In Japan, where the prevalence of hepatitis B and hepatitis C is similar, the incidence of hepatocellular carcinoma is higher in patients with hepatitis C compared to hepatitis B (10.4% vs. 3.9%). The pathogenesis of hepatocellular carcinomain the presence of hepatitis B virus may be due toincreased cell turnover from chronic liver disease, or a combination of processes specific to the hepatitis B virus. These may include integration of the hepatitis B DNA genome into the host genome, thereby disrupting the regulatory elements of cell cycling, or via transactivation of host oncogenes by either HBx protein ora truncated protein derived from pre-S2/S region of hepatitis B genome. The pathogenesis of hepatocellular carcinoma in hepatitis C is less understood. It is possiblethat some of these patients had previous exposure to hepatitis B virus (Ahmet Gurakar et al 2013).

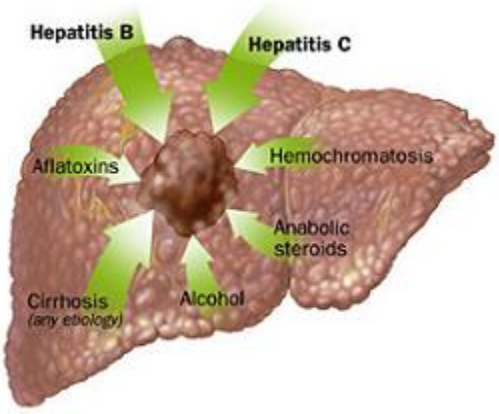

Figure 2.3 Causes of hepatocellular carcinoma

Cirrhosis, irrespective of its etiology , is a risk factor for the development of hepatocellular carcinoma. The risk is 3–4 times higher in patients with cirrhosis compared to those with chronic hepatitis in a given population. An increase in hepatocellular proliferation maylead to the activation of oncogenes and mutation of tumor suppressor genes. These changes, in turn, may initiate hepatocarcinogeneses. In low-incidence areas, more than 90% of patients with hepatocellular carcinoma have underlying cirrhosis. However, the presence of cirrhosis is less (approximately 80%) in high-incidence areas, which is probably related to vertical transmission of hepatitis B virus in these areas (Figure 2.3) (Ahmet Gurakar et al 2013).

Other Factors: Other etiological factors affecting disease incidence include aflatoxins, alcohol, hemochromatosis , and anabolic steroid use (Figure 2.3). Exposure to dietary carcinogenic aflatoxins, produced by Aspergillus parasiticus and Aspergillus flavus, is common in certain regions of Southeast Asia and sub-Saharan Africa. Hepatitis B is also common in these areas. The relative contribution of aflatoxins and the hepatitis B virus to the pathogenesis of hepatocellular carcinoma in these parts of the world are poorly understood. In patients with hepatitis C viral infection, alcohol has been found to be another contributing factor. Whether this is related to a

more aggressive disease due to a combination of hepatitis C virus and alcohol, or whether alcohol is an independent factor remains unknown. The incidence of hepatocellular carcinoma in patients with hemochromatosis can be as high as 45%, and often the tumor is multifocal (Ahmet Gurakar et al 2013).

2.2 Diagnosis of HCC:

2.2.1 Alpha-Fetoprotein (AFP) :

Alpha-fetoprotein levels may be assessed by a blood test. Alpha-fetoprotein (AFP) is a tumor marker that is elevated in 60–70% of patients with hepatocellular carcinoma. Normally, levels of AFP are below 10 ng/ml, but marginal elevations (10–100) are common in patients with chronic hepatitis. However, all patients with elevated AFP should be screened (abdominal ultrasound, CT scan or MRI) for hepatocellular carcinoma, especially if there has been an increase from baseline levels. In our experience, a steadily rising AFP is almost diagnostic of hepatocellular carcinoma. The specificity of AFP is very high when the levels are above 400 ng/ml. Undifferentiated teratocarcinoma and embryonal cell carcinoma of the testis or ovary may give false-positive results and should be considered in the differential diagnosis of elevated AFP (Ahmet Gurakar et al 2013).

The doubling time of AFP is around 60–90 days. Therefore, it may be advisable to check AFP every 3–4 months to screen high-risk cirrhotic patients (hepatitis C, hepatitis B, and hemochromatosis) for hepatocellular carcinoma.

2.2.2 Radiographic Diagnosis:

The diagnostic accuracy of ultrasound, CT , magnetic resonance imaging (MRI) and angiography is dependent on a number of variables: expertise of the operator (especially with ultrasound), sophistication of equipment and technique, presence of cirrhosis and, most importantly, experience

of the interpreter. For small tumors (<2 cm), the diagnostic accuracy ranges from 60–80%. The diagnostic accuracy increases significantly with an increase in tumor size, ultimately reaching 100% with very large tumors with all modalities (Figure 2.4).

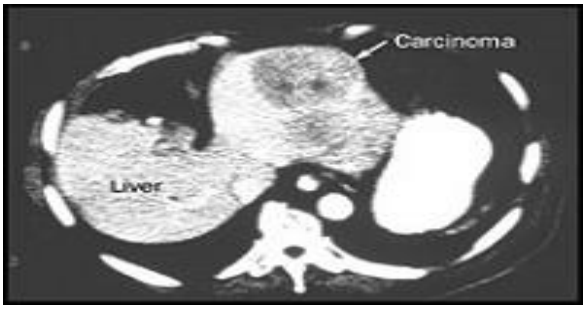

Figure 2.4.Computed tomography (CT) scan of hepatocellular carcinoma

Liver Biopsy and Histological Grading Liver biopsy is indicated when diagnosis is in doubt (Figure 2.4). If AFP is significantly elevated and a tumor is seen in the liver, it is reasonable to assume a diagnosis of hepatocellular carcinoma and a liver biopsy is not warranted (Ahmet Gurakar et al 2013).

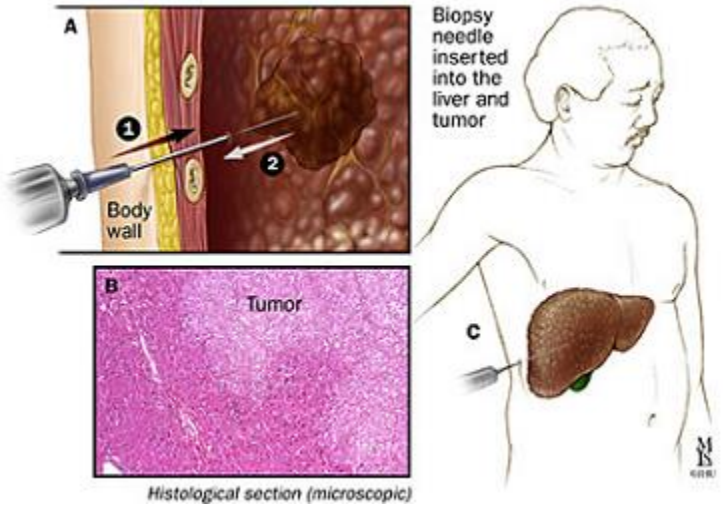

Figure 2.5 A, Biopsy of focal tumor; B, histological appearance; C, percutaneous approach to the liver

The World Health Organization has suggested that hepatocellular carcinoma might be classified into histological types based on the structural organization of tumor cells: trabecular or sinusoidal type, pseudoglandular or acinar type, and compact or scirrhous sclerosing agent type. The tumor could also be graded based on the degree of cell differentiation into well, moderately, and poorly differentiated (Ahmet Gurakar et al 2013).

2.3 Therapy of HCC:

The optimal management of hepatocellular carcinoma depends on a variety of factors including the size, number, and distribution (unilobar vs. bilobar) of tumors, the relationship of the tumor to hepatic vasculature, the status of distant metastases, the severity of liver disease (Child-Pugh score), the suitability of the patient for liver transplantation, the functional status of the patient, and local expertise. The mean survival of symptomatic patients with hepatocellular carcinoma is approximately 2–3 months. The doubling time of the tumor size is 2–3 months. Optimal management should attempt to prolong without compromising quality of life (Ahmet Gurakar et al 2013).

2.4 Computed Radiography:

Over more than 30 years of advances in technologies, including x-ray generation, filtration design, detector, firmware, and post-processing, CT has developed into a medical imaging modality with the capability of obtaining excellent resolution for both high contrast and low contrast tasks, as well as the capability to perform volumetric imaging by the implementation of multi-row detectors (MDCT). It has been a major diagnostic tool and has been impacting patient healthcare throughout the entire world. Today CT is routinely used as a key component in Radiology and Oncology departments for many areas of medical applications. To name a few, within Radiology department, it is used in head scans to detect infarction, hemorrhage, or trauma; it is used in thoracic scans for

detecting both acute and chronic changes in the lung parenchyma; it is used in Cardiology to diagnose cardiovascular diseases; it is used in abdomen or pelvic scans to determine the stage of cancer and to follow progress; it is also used in extremity scans to image complex fractures, especially one around joints because of its ultra-high spatial resolution. Within Oncology department, CT is used to obtain attenuation properties for body tissues in order to perform necessary calculations of radiation dose distribution in treatment planning (Mettler, et al 2008).

CT scanners use x-ray tubes to generation photons. In this process, electrons are emitted from cathode via thermionic emission and are accelerated within the tube towards anode driven by the potential difference between the cathode and the anode. The highly energetic electrons then interact with matter (usually tungsten) and convert their kinetic energy into heat and electromagnetic radiation (photons) through the process of bremsstrahlung. Figure 1 shows the physical look of the anode. The fluence of photons depends on kVp and mAs. kVp is defined as the peak tube potential between the cathode and the anode. It determines the highest energy of photons within the beam. mAs is the multiplication of tube current (the rate of the charge of electrons from the cathode to the anode) and exposure time. mAs is proportional to the fluence of the x-ray beam (Mettler, et al 2008).

During the CT scan a patient lies on the table while the x-ray tube and the detector ring spin in the gantry in a very fast speed (as fast as 0.27s/rotation for certain manufacturer). Fan shaped beams are used in modern CT scanners as shown in figure (2.2) There are two different scan modes with respect to the pattern of the movement of the bed: axial scan and helical scan. In axial scan, the bed moves incrementally after every rotation so the anatomy is captured section by section; in helical scan, the bed moves continuously while the tube and detector are rotating.

Under helical scan mode, pitch is defined as the advance of the table in a rotation divided by the nominal collimation width in z direction. Helical scan was introduced in 1990s and it has dramatically increased the time efficiency of CT scans.

The number of CT scans in United States has increase from 18.3 million in 1993 to 62.0 million in 2006, with an estimated annual growth rate of 10% 5,6 . Especially since the introduction of MDCT in mid 1990s, the use of CT has increased dramatically due to its improved capacity. In clinical practice, CT exams consists 15% of the total number of radiological imaging procedures, but it contributes to 50% of the population radiation exposure from medical procedures, and it contributes to 25% of the population radiation exposure from all sources, including background radiation. This has lead to concerns about the potential risks of radiation hazards to patients (Mettler, 2008).

Imaging is basically a process consisting of two distinct stages: image recording and image display (Wagner 1983, ICRU 1996). This division is especially important in digital imaging, where these stages are clearly separate. In digital imaging the image recording stage (or the image data stage) determines the information that has been captured in the image data and can be analyzed in terms of the pixel values. Performing actual physical measurements of the display stage is cumbersome and its evaluation is for the most part done mainly visually.

2.5 Biomedical Image Processing:

By the increasing use of direct digital imaging systems for medical diagnostics, digital image processing becomes more and more important in health care. In addition to originally digital methods, such as Computed Tomography (CT) or Magnetic Resonance Imaging (MRI), initially analogue imaging modalities such as endoscopy or radiography are nowadays equipped with digital sensors (Deserno et al 2007).

Digital images are composed of individual pixels (this acronym is formed from the words “picture” and “element”), to which discrete brightness or color values are assigned. They can be efficiently processed, objectively evaluated, and made available at many places at the same time by means of appropriate communication networks and protocols, such as Picture Archiving and Communication Systems (PACS) and the Digital Imaging and Communications in Medicine (DICOM) protocol, respectively. Based on digital imaging techniques, the entire spectrum of digital image processing is now applicable in medicine (Deserno et al 2007).

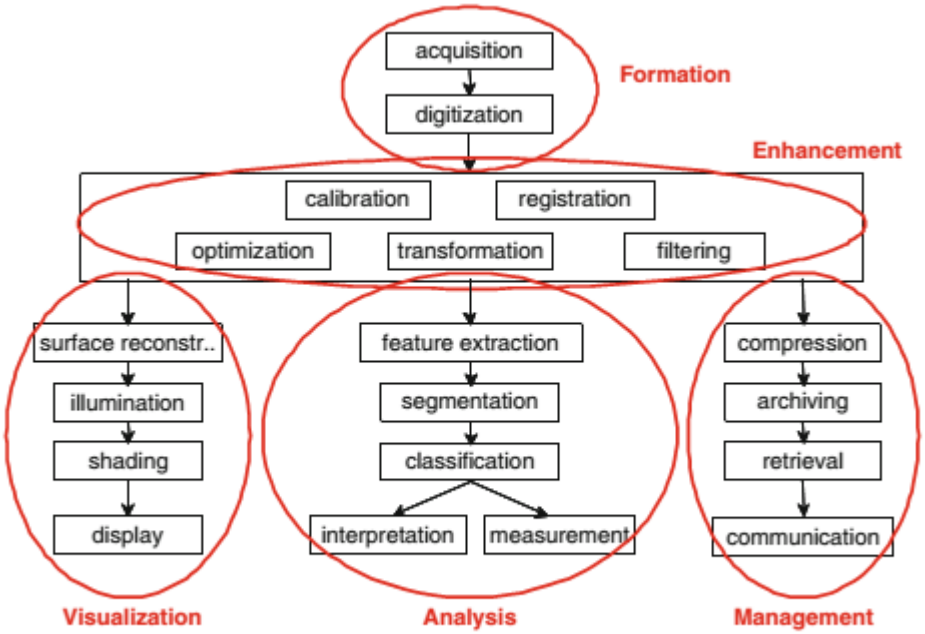

Fig.2.6 .Modules of image processing, In general, image processing covers four main areas: image formation, visualization, analysis, and management. The algorithms of image enhancement can be assigned as pre- and postprocessing in all areas .

2.5.1 Steps of Image Processing :

The commonly used term "biomedical image processing" means the provision of digital image processing for biomedical sciences. In general, digital image processing covers four major areas (Figure 2.6) :

- Image formation includes all the steps from capturing the image to forming a digital image matrix.
- Image visualization refers to all types of manipulation of this matrix, resulting in an optimized output of the image.
- Image analysis includes all the steps of processing, which are used for quantitative measurements as well as abstract interpretations of biomedical images. These steps require a priori knowledge on the nature and content of the images, which must be integrated into the algorithms on a high level of abstraction. Thus, the process of image analysis is very specific, and developed algorithms can be transferred rarely directly into other application domains.
- Image management sums up all techniques that provide the efficient storage, communication, transmission, archiving, and access (retrieval) of image data. Thus, the methods of telemedicine are also a part of the image management .

In contrast to image analysis, which is often also referred to as high-level image processing, low-level processing denotes manual or automatic techniques, which can be realized without a priori knowledge on the specific content of images. This type of algorithms has similar effects regardless of the content of the images. For example, histogram stretching of a radiograph improves the contrast as it does on any holiday photograph. Therefore, low-level processing methods are usually available with programs for image enhancement (Deserno et al 2007).

2.6 Texture analysis:

Texture analysis is presented here as a useful computational method for discriminating between pathologically different regions on medical images because it has been proven to perform better than human eyesight at discriminating certain classes of texture (Julesz, 1975).

2.6.1 First-Order Statistical Texture Analysis

First-order texture analysis measures use the image histogram, or pixel occurrence $0 \leq i \leq N_g - 1$ probability, to calculate texture. The main advantage of this approach is its simplicity through the use of standard descriptors (e.g. mean and variance) to characterise the data (Press, 1998). However, the power of the approach for discriminating between unique textures is limited in certain applications because the method does not consider the spatial relationship, and correlation, between pixels. For anysurface, or image, grey-levels are in the range where N_g is the total number of distinct grey-levels , If (N_i) is the number of pixels with intensity i and M is the total number of pixels in an image, it follows that the histogram, or pixel occurrence probability, is given by,

$$P(i) = \frac{N(i)}{M}.$$

In general seven features commonly used to describethe properties of the image histogram, and therefore image texture, are computed. These are: mean; variance; coarseness; skewness; kurtosis; energy; and entropy.

2.6.2 Second-Order Statistical Texture Analysis

The human visual system cannot discriminate between texture pairs with matching second order statistics (see Fig. 2.6) (Julesz et al, 1975). The first machine-vision framework for calculating second-order or pixel co-occurrence texture information was developed for analysing aerial photography images (Haralick et al., 1973). In this technique pixel co-occurrence matrices, which are commonly referred to as grey-tone spatial dependence matrices (GTSDM), are computed. The entries in a GTSDM are the probability of finding a pixel with grey-level i at a distance d and angle α from a pixel with a grey-level j. This may be written more formally as $P(I,j:d,\alpha)$. An essential component of this framework is that each pixel has eight nearest-neighbours connected to it, except atthe periphery. As a result four GTSDMs are required to describe the texture content in thehorizontal ($P_H=0^0$), vertical ($P_V=90^0$), right- ($P_{RD}=45^0$), and left-diagonal ($P_{LD}=135^0$), directions. This is illustrated in Fig. 8

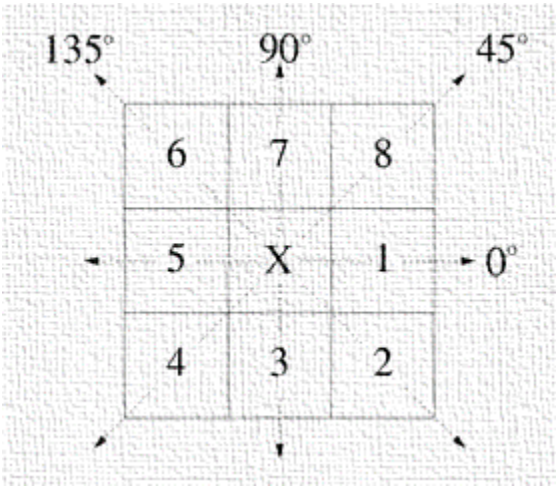

Fig. 2.7. Eight nearest-neighbour pixels used in the GTSDM framework to describe pixel connectivity. Cells 1 and 5 show the horizontal (P_H) 4 and 8 the right-diagonal (P_{RD}), 3 and 7 the vertical (P_V), and 2 and 6 the left-diagonal (P_{LD}) nearest-neighbours.

An example of the calculation of a horizontal co-occurrence matrix (P_H) on a 4×4 image containing four unique grey-levels is shown in Fig.6. A complete representation of image texture is contained in the co-occurrence matrices calculated in the four directions.

Extracting information from these matrices using textural features, which are sensitive to specific elements of texture, provides unique information on the structure of the texture being investigated. Haralick et al., proposed a set of 14 local features specifically designed for this purpose (Haralick et al., 1973). In practice the information provided by certain features may be highly correlated or of limited practical use. A feature selection strategy is therefore useful with this approach to take account of redundant, or irrelevant, information.

This is discussed in more detail in section 5. It is also interesting to note that prior to any processing the GTSDMs, which are symmetric, can provide some useful information on the characteristics of the image being studied. For example, the co-occurrence matrix entries for a coarse texture will be heavily focused along the diagonals relative to the distance d between the pixels studied.

0	2	2	2
0	3	2	2
1	2	2	2
3	0	3	0

(P_H)

Grey-Level	0^0	0	1	2	3
	0	0	0	1	4
	1	0	0	1	0
	2	1	1	10	1
	3	4	0	1	0

Fig. 2.8. Simple example demonstrating the formation of a co-occurrence matrix from an image. Left, 4*4 image with four unique grey-levels. Right, the resulting horizontal co-occurrence matrix (P_H).

Angular second moment

$$f_1 = \sum_{i=1}^{N_q} \sum_{j=1}^{N_q} p'(i,j)^2.$$

Contrast,

$$f_2 = \sum_{i=0}^{Nq-1} n^2 \left[\sum_{i=1}^{Nq} \sum_{j=1}^{Nq} p'(i,j) \right]_{i-j=n}.$$

Correlation,

$$f_3 = \sum_{i=1}^{N_q} \sum_{j=1}^{N_q} \frac{(i-\mu_x)(j-\mu_y)p'(i,j)}{\sigma_x \sigma_y},$$

where, N_q is the number of distinct grey-levels in the input and, μ_x, μ_y, σ_X, are the means and standard deviations of P(i,j) . Throughout, P(i,j)= P(i,j)/R where P(i,j) is (P_H,P_V,P_{LD},P_{RD}) and R is the maximum number of resolution cells in a GTSDM.

2.6.3 Higher-Order Statistical Texture Analysis

The grey-level run length method (GLRLM) is based on the analysis of higher-order statistical information (Galloway, 1975). In this approach GLRLMs contain information on the run of a particular grey-level, or grey-level range, in a particular direction. The number of pixels contained within the run is the run-length.

A coarse texture will therefore be dominated by relatively long runs whereas a fine texture will be populated by much shorter runs. The number of runs r with gray-level i , or lying within a grey-level range i , of runlength j in a direction α is denoted by R(α) = {r(I,j)/α} .

This is analogous to the GTSDM technique (Haralick et al., 1973) as four GTRLMs are commonly used to describe texture runs in the directions ($0^0, 90^0, 180^0$ AND 135^0) . on linearly adjacent pixels. An example of the calculation of a horizontal GLRLM is shown in Fig. 2.10.

0	1	2	2
0	3	2	2
1	2	2	2
3	0	3	0

Grey-Level	Run-Length			
	0^0	1	2	3	4
0	4	0	0	0
1	2	0	0	0
2	0	2	1	0
3	3	0	0	0

Fig. 2.10 Simple example demonstrating the formation of a GLRLM. Left, 4*4 image with four unique grey-levels. Right, the resulting GLRLM in the direction 0^0.

A set of seven numerical texture measures are computed from the GTRLMs. Three of these measures are presented here to illustrate the computation of feature information using this framework.

Short Run Emphasis,

$$f_{SR} = \frac{1}{T_R} \sum_{i=0}^{N_g-1} \sum_{j=1}^{N_r} \frac{r'(i,j \mid \alpha)}{j^2}.$$

Long Run Emphasis,

$$f_{LR} = \frac{1}{T_R} \sum_{i=0}^{N_g-1} \sum_{j=1}^{N_r} j^2 r'(i,j \mid \alpha).$$

Grey-Level Distribution,

$$f_{GD} = \frac{1}{T_R} \sum_{i=0}^{N_g-1} \left[\sum_{j=1}^{N_r} r'(i,j \mid \alpha) \right]^2,$$

Where Ng is the maximum number of grey-levels, Nr is the number of different run lengths in the matrix and,

$$T_R = \sum_{i=0}^{N_g-1} \sum_{j=1}^{N_r} r'(i,j \mid \alpha).$$

T_R serves as a normalizing factor in each of the run length equations.

2.7 Fourier Power Spectrum:

Two-dimensional transforms have been used extensively in image processing to tackle problems such as image description and enhancement (Pratt, 1978). Of these, the Fourier transform is one of the most widely used (Gonzalez and Woods, 2001). Fourier analysis can be used to study the properties of textured scenes, for example the power spectrum reveals information on the coarseness/fineness (periodicity) and directionality of a texture. Texture directionality is preserved in the power spectrum because it allows directional and nondirectional components of the texture to be distinguished (Bajscy, 1973). These observations have given rise to two powerful approaches for extracting texture primitives from the Fourier power spectrum, namely, ring and wedge filters. Working from the origin of the power spectrum the coarseness/fineness is measured between rings of inner radius r_1 and r_2 .

The size of the rings can be varied according to the application. The directionality of the texture is found by measuring the average power over wedge-shaped regions centred at the origin of the power spectrum. The size of the wedge $\phi_w=\phi_1-\phi_2$ depends upon the application. Fig. 8 illustrates the extraction of ring and wedge filters from the Fourier power spectrum of a 32×32 test image consisting of black pixels everywhere except for a 3×3 region of white pixels centred at the origin.

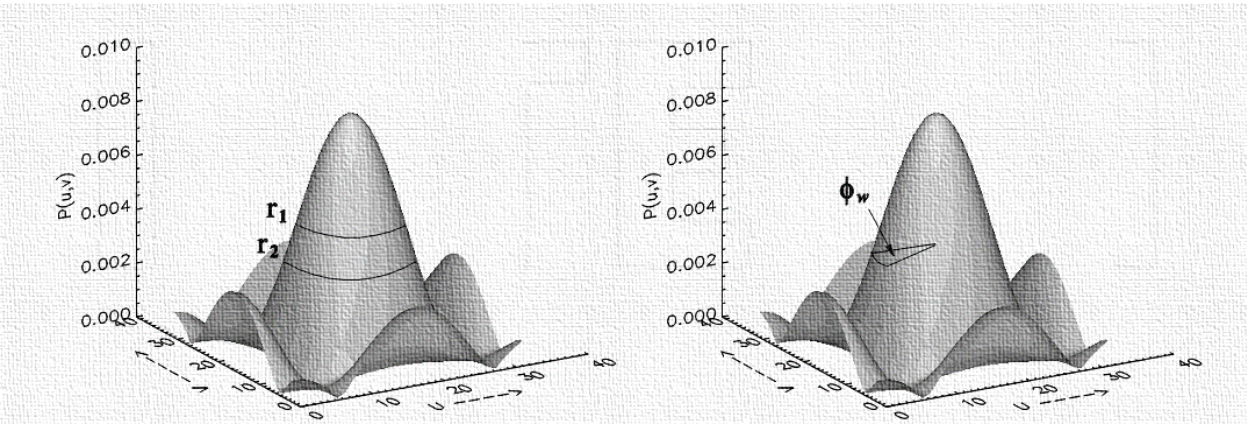

Fig. 2.11 Fourier power spectrum showing the extraction of ring and wedge filters. The spectrum was generated on a 32×32 test image consisting of black pixels everywhere except for a 3×3 region of white pixels centred at the origin.

In image analysis the Fourier transform P(u,v) is considered in its discrete form and the power spectrum P(u,v) is calculated from,

$$P(u,v)=|F(u,v|^2.$$

The average power contained in a ring centred at the origin with inner and outer radii

r_1 and r_2 respectively, is given by the summation of the contributions along the direction ϕ.

$$P(r) = 2\sum_{\phi=0}^{\pi} P(r,\phi).$$

he contribution from a wedge of size ϕ_w is found from summation of the radial components within the wedge boundaries. That is,

$$P(\phi_w) = \sum_{r=0}^{n/2} P(r,\phi),$$

where n is the window size.

2.8 Guide to Wavelets:

Fourier theory its a signal can be expressed as the sum of a, possibly infinite, series of sines and cosines. This sum is also referred to as a Fourier expansion. The big disadvantage of a Fourier expansion however is that it has only frequency resolution and no time resolution. This means that although we might be able to determine all the frequencies present in a signal, we do not know when they are present. To overcome this problem in the past decades several solutions have been developed which are more or less able to represent a signal in the time and frequency domain at the same time (she et al 1996).

The idea behind these time-frequency joint representations is to cut the signal of interest into several parts and then analyze the parts separately.

The problem here is that cutting the signal corresponds to a convolution between the signal and the cutting window. Since convolution in the time domain is identical to multiplication in the frequency domain and since the Fourier transform of a Dirac pulse contains all possible frequencies the frequency components of the signal will be smeared out all over the frequency

axis. In fact this situation is the opposite of the standard Fourier transform since we now have time resolution but no frequency resolution whatsoever (she et al 1996).

The underlying principle of the phenomena just described is Heisenberg's uncertainty principle, which, in signal processing terms, states that it is impossible to know the exact frequency and the exact time of occurrence of this frequency in a signal. In other words, a signal can simply not be represented as a point in the time-frequency space. The uncertainty principle shows that it is very important how one cuts the signal (she 96).

The wavelet transform or wavelet analysis is probably the most recent solution to overcome the shortcomings of the Fourier transform. In wavelet analysis the use of a fully scalable modulated window solves the signal-cutting problem. The window is shifted along the signal and for every position the spectrum is calculated. Then this process is repeated many times with a slightly shorter (or longer) window for every new cycle. In the end the result will be a collection of time-frequency representations of the signal, all with different resolutions. Because of this collection of representations, we can speak of a multiresolution analysis. In the case of wavelets we normally do not speak about time-frequency representations but about time-scale representations, scale being in a way the opposite of frequency, because the term frequency is reserved for the Fourier transform (she 96).

2.8.1 Wavelet properties

The most important properties of wavelets are the admissibility and the regularity conditions and these are the properties which gave wavelets their name. It can be shown [She96] that square integrable functions 5(*t*) satisfying the *admissibility condition*,

$$\int \frac{|\Psi(\omega)|^2}{|\omega|} d\omega < +\infty ,$$

can be used to first analyze and then reconstruct a signal without loss of information. The admissibility condition implies that the Fourier transform of 5(*t*) vanishes at the zero frequency, i.e.

$$|\Psi(\omega)|^2\Big|_{\omega=0} = 0 .$$

This means that wavelets must have a band-pass like spectrum. This is a very important observation, which we will use later on to build an efficient wavelet transform.

A zero at the zero frequency also means that the average value of the wavelet in the time domain must be zero,

$$\int \psi(t)dt = 0 ,$$

and therefore it must be oscillatory. In other words, 5(*t*) must be a *wave*.

The time-bandwidth product of the wavelet transform is the square of the input signal and for most practical applications this is not a desirable property. Therefore one imposes some additional conditions on the wavelet functions in order to make the wavelet transform decrease quickly with decreasing scale s. These are the regularity conditions and they state that the wavelet function should have some smoothness and concentration in both time and frequency domains. Regularity is a quite complex concept and we will try to explain it a little using the concept of vanishing moments.

If we expand the wavelet transform we get [She96]:

$$\gamma(s,0) = \frac{1}{\sqrt{s}}\left[\sum_{p=0}^{n} f^{(p)}(0)\int \frac{t^p}{p!}\psi\left(\frac{t}{s}\right)dt + O(n+1)\right] .$$

Here $f^{(p)}$ stands for the p^{th} derivative of f and $''(n+1)$ means the rest of the expansion. Now, if we define the *moments* of the wavelet by M_p,

$$M_p = \int t^p \psi(t) dt ,$$

then into the finite development

$$\gamma(s,0) = \frac{1}{\sqrt{s}} \left[f(0) M_0 s + \frac{f^{(1)}(0)}{1!} M_1 s^2 + \frac{f^{(2)}(0)}{2!} M_2 s^3 + \ldots + \frac{f^{(n)}(0)}{n!} M_n s^{n+1} + O(s^{n+2}) \right].$$

From the admissibility condition we already have that the 0^{th} moment $M_0 = 0$ so that the first term in the right-hand side is zero. If we now manage to make the other moments up to M_n zero as well, then the wavelet transform coefficients $\gamma(s,-)$ will decay as fast as s^{n+2} for a smooth signal $f(t)$. This is known in literature as the vanishing moments[3] or *approximation order*. If a wavelet has N vanishing moments, then the approximation order of the wavelet transform is also N. The moments do not have to be exactly zero, a small value is often good enough. In fact, experimental research suggests that the number of vanishing moments required depends heavily on the application [Cal et al 1996].

Summarizing, the admissibility condition gave us the wave, regularity and vanishing moments gave us the fast decay or the *let*, and put together they give us the wavelet. More about regularity can be found for instance in [Bur et al 1998] and [Dau et al992].

2.8.2 The continuous wavelet transform

The wavelet analysis described in the introduction is known as the *continuous wavelet transform* or *CWT*. More formally it is written as:

$$\gamma(s,\tau) = \int f(t) \psi^*_{s,\tau}(t) dt ,$$

where * denotes complex conjugation. This equation shows how a function $f(t)$ is decomposed into a set of basis functions $\Psi_{s,-}(t)$, called the wavelets. The variables s and – are the new dimensions, scale and translation, after the wavelet transform. For completeness sake equation gives the inverse wavelet transform. I will not expand on this since we are not going to use it:

$$f(t) = \iint \gamma(s,\tau)\psi_{s,\tau}(t)d\tau ds .$$

The wavelets are generated from a single basic wavelet 5(t), the so-called *mother wavelet*, by scaling and translation:

$$\psi_{s,\tau}(t) = \frac{1}{\sqrt{s}}\psi\left(\frac{t-\tau}{s}\right).$$

In s is the scale factor, – is the translation factor and the factor $s^{-1/2}$ is for energy normalization across the different scales (cal et al 1996).

This is a difference between the wavelet transform and the Fourier transform, or other transforms. The theory of wavelet transforms deals with the general properties of the wavelets and wavelet transforms only. It defines a framework within one can design wavelets to taste and wishes.

2.8.3 Discrete wavelets

the wavelet transform is calculated by continuously shifting a continuously scalable function over a signal and calculating the correlation between the two. It will be clear that these scaled functions will be nowhere near an orthogonal basis and the obtained wavelet coefficients will therefore be highly redundant. For most practical applications we would like to remove this redundancy.

Even without the redundancy of the CWT we still have an infinite number of wavelets in the wavelet transform and we would like to see this number reduced to a more manageable count. This is the second problem we have.

The third problem is that for most functions the wavelet transforms have no analytical solutions and they can be calculated only numerically or by an optical analog computer. Fast algorithms are needed to be able to exploit the power of the wavelet transform and it is in fact the existence of these fast algorithms that have put wavelet transforms where they are today.

As mentioned before the CWT maps a one-dimensional signal to a two-dimensional time-scale joint representation that is highly redundant. The time-bandwidth product of the CWT is the square of that of the signal and for most applications, which seek a signal description with as few components as possible, this is not efficient. To overcome this problem *discrete wavelets* have been introduced. Discrete wavelets are not continuously scalable and translatable but can only be scaled and translated in discrete steps. This is achieved by modifying the wavelet representation to create [Dau92]

$$\Psi_{j,k}(t) = \frac{1}{\sqrt{s_0^j}} \Psi\left(\frac{t - k\tau_0 s_0^j}{s_0^j} \right).$$

Although it is called a discrete wavelet, it normally is a (piecewise) continuous function. In (10) j and k are integers and $s_0 > 1$ is a fixed dilation step. The translation factor τ_0 depends on the dilation step. The effect of discretizing the wavelet is that the time-scale space is now sampled at discrete intervals. We usually choose $s_0 = 2$ so that the sampling of the frequency axis corresponds to *dyadic sampling*. This is a very natural choice for computers, the human ear and music for instance. For the translation factor we usually choose $\tau_0=1$ so that we also have dyadic

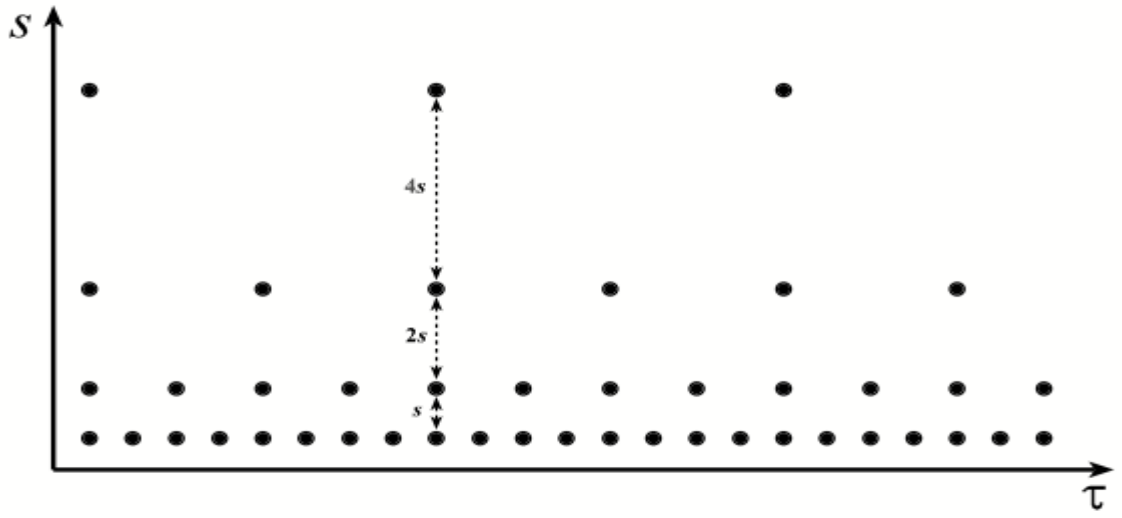

Figure 2.12 *Localization of the discrete wavelets in the time-scale space on a dyadic grid.*

When discrete wavelets are used to transform a continuous signal the result will be a series of wavelet coefficients, and it is referred to as the *wavelet series decomposition*. An important issue in such a decomposition scheme is of course the question of reconstruction. It is all very well to sample the time-scale joint representation on a dyadic grid, but if it will not be possible to reconstruct the signal it will not be of great use. As it turns out, it is indeed possible to reconstruct a signal from its wavelet series decomposition. In [Dau92] it is proven that the necessary and sufficient condition for stable reconstruction is that the energy of the wavelet coefficients must lie between two positive bounds, i.e.

$$A\|f\|^2 \le \sum_{j,k} \left|\left\langle f, \Psi_{j,k} \right\rangle\right|^2 \le B\|f\|^2,$$

Where f^2 is the energy of $f(t)$, $A > 0$, $B <$ and A, B are independent of $f(t)$. When equation is satisfied, the family of basis functions $5_{j,k}(t)$ with j, k Z is referred to as a *frame* with frame bounds A and B. When $A = B$ the frame is *tight* and the discrete wavelets behave exactly like an orthonormal basis. When A ¹ B exact reconstruction is still possible at the expense of a *dual frame*. In a dual frame discrete wavelet transform the decomposition wavelet is different from

the reconstruction wavelet.

We will now immediately forget the frames and continue with the removal of all redundancy from the wavelet transform. The last step we have to take is making the discrete wavelets orthonormal. This can be done only with discrete wavelets. The discrete wavelets can be made orthogonal to their own dilations and translations by special choices of the mother wavelet, which means:

$$\int \psi_{j,k}(t)\psi^{*}_{m,n}(t)dt = \begin{cases} 1 & if \quad j=m \quad and \quad k=n \\ 0 & otherwise \end{cases}.$$

An arbitrary signal can be reconstructed by summing the orthogonal wavelet basis functions, weighted by the wavelet transform coefficients [She96]:

$$f(t) = \sum_{j,k} \gamma(j,k)\psi_{j,k}(t).$$

Equation shows the inverse wavelet transform for discrete wavelets, which we had not yet seen. Orthogonality is not essential in the representation of signals. The wavelets need not be orthogonal and in some applications the redundancy can help to reduce the sensitivity to noise [She96] or improve the *shift invariance* of the transform [Bur et al 1998]. This is a disadvantage of discrete wavelets: the resulting wavelet transform is no longer shift invariant, which means that the wavelet transforms of a signal and of a time-shifted version of the same signal are not simply shifted versions of each other.

2.9 Previous Study:

Daniel Smutek et al (2011) is developing a computer-aided diagnostic (CAD) system for focal liver lesions in CT images. The texture analysis methods are used for the classification of hepatocellular cancer and liver cysts. CT contrast enhanced images of 20 adult subjects with hepatocellular carcinoma or with non-parasitic solitary liver cyst were used as entry data. A total number of 130 spatial and second-order probabilistic texture features were computed from the images. Ensemble of Bayes classifiers was used for the tissue classification.

Classification success rate was as high as 100% when estimated by leave-one-out method. This high success rate was achieved with as few as one optimal descriptive feature representing the average deviation of horizontal curvature computed from original pixel gray levels. This promising result allows further amplification of this approach in distinguishing more types of liver diseases from CT images.

Samia A. F. Ahmed et al (2014) in this study A new approach to texture characterization from dynamic CT scans of the liver is presented. This study was aimed to use the texture analysis and classification methods to characterize the hepatocellular carcinoma (HCC), liver and other abdominal regions in CT images using image processing program (IDL, interactive data language). Tri-phasic Multi detectors CT with contrast enhanced

images of 200 adult subjects with hepatocellular carcinoma were used as entry data. Tiff format was created as IDL variables and then using 3x3 window the image was scanned and based on the image histogram the selected feature also called FOS was calculated using this window. Linear discriminant analysis was used for the tissue classification. The study found that the HCC texture reveal a different

underlying pattern compared to the liver and other abdominal tissues with classification sensitivity and specificity 96.5% and 86.6% respectively, and the combination of the texture features throughout the different tri-phasic image phases provide the highest predictive overall accuracy of 89.1 % using linear discriminant analysis.

in this study carried by Gunasundari S et al (2013) studied Liver diseases by considered seriously because liver is a vital organ to human beings. Computer aided liver analysis is atechnique that can help radiologists to accurately identify diseases that can help in reducing the risk of liver surgery.

The computer aided diagnosis (CAD) system consists of the segmentation of liver and lesion, extraction of features from a lesion and characterization of liver diseases by means of a classifier. In the last decade, the use of many segmentation techniques and classifier systems have been proposed by many authors with the intention to increase the performance of CAD systems This article focuses on various textural analysis methods used so far for the classification of liver diseases from abdominal Computed Tomography scans. It reviews the techniques and results of the various methods are analyzed and summarized. The future direction for the research is also discussed.

Characterization of CT Liver Lesions Based on Texture Features and a Multiple Neural Network Classification Scheme S. Gr. Mougiakakou et al (2003) using a Computer Aided Diagnosis (CAD) system for the characterization of hepatic tissue from Computed Tomography (CT) images is presented. Regions of Interest (ROI's) corresponding to normal liver, cyst, hemangioma, and hepatocellular carcinoma, are drawn by an experienced radiologist on abdominal non-enhanced CT images. For each ROI, five distinct sets of texture features are extracted using the following

methods: first order statistics, spatial gray level dependence matrix, gray level difference method, Laws' texture energy measures, and fractal dimension measurements. If the dimensionality of a feature set is greater than a predefined threshold, feature selection based on a Genetic Algorithm (GA) is applied. Classification of the ROI is then carried out by a system of five neural networks (NNs), each using as input one of the above feature sets. The members of the NN system (primary classifiers) are 4-class NNs trained by the backpropagation algorithm with adaptive learning rate and momentum. The final decision of the CAD system is based on the application of a voting scheme across the outputs of the individual NNs. The multiple classification scheme using the five sets of texture features results in significantly enhanced performance, as compared to the classification performance of the individual primary classifiers.

M. Gletsos et al (2001) in different study using a computer-aided diagnostic system for the classification of hepatic lesions from Computed Tomography (CT) images is presented. Regions of Interest (ROI's) taken from non-enhanced CT images of normal liver, hepatic cysts, hemangiomas, and hepatocellular carcinomas (a total of 147 samples), have been used as input to the system.

The system consists of two levels: the feature extraction and the classification levels. The feature extraction level calculates the average grey scale and 48 texture characteristics, which are derived from the spatial grey-level co-occurrence matrices, obtained from the ROI's. The classifier level consists of three sequentially placed feed-forward Neural Networks (NN's), which are activated sequentially. The first NN classifies into normal or pathological liver regions. The pathological liver regions are classified by the second NN into cysts or "other disease". The third NN classifies "other disease" into hemangiomas and hepatocellular carcinomas. In order to enhance the performance of the classifier and improve the execution time, the dimensionality of the initial

feature vector has been reduced using the sequential forward floating selection method for each individual NN input vector. A total classification rate of 98% has been achieved.

Paola Campadelli (2009) this work has been devoted to the development of semi-automatic and automatic techniques for the analysis of abdominal CT images. Some of the current interests are the automatic diagnosis of liver, spleen, and kidney pathologies and the 3D volume rendering of the abdominal organs. The first and fundamental step in all these studies is the automatic organs segmentation, that is still an open problem. In this paper we propose our fully automatic system that employs a hierarchical gray level based framework to segment heart, bones (i.e. ribs and spine), liver and its blood vessels, kidneys, and spleen. The overall system has been evaluated on the data of 100 patients, obtaining a good assessment both by visual inspection by three experts, and by comparing the computed results to the boundaries manually traced by experts.

In a novel study carried by ROBERT M. HARALICK, et al (1973) Texture is one of the important characteristics used in identifying objects or regions of interest in an image, whether the image be a photomicrograph, an aerial photograph, or a satellite image. This paper describes some easily computable textural features based on graytone spatial dependancies, and illustrates their application in category identification tasks of three different kinds of image data: photomicrographs of five kinds of sandstones, 1:20 000 panchromatic aerial photographs of eight land-use categories, and Earth Resources Technology Satellite (ERTS) multispecial imagery containing seven land-use categories. We use two kinds of decision rules: one for which the decision regions are convex polyhedra (a piecewise linear decision rule), and one for which the decision regions are rectangular parallelpipeds (a min-max decision rule). In each experiment the data set was divided into two parts, a training set and a test set. Test set identification accuracy is

89 percent for the photomicrographs, 82 percent for the aerial photographic imagery, and 83 percent for the satellite imagery. These results indicate that the easily computable textural features probably have a general applicability for a wide variety of image-classification applications.

M. Gletsos et al (2001) in this study they using a computer-aided diagnostic system for the classification of hepatic lesions from Computed Tomography (CT) images is presented. Regions of Interest (ROI's) taken from non-enhanced CT images of normal liver, hepatic cysts, hemangiomas, and hepatocellular carcinomas (a total of 147 samples), have been used as input to the system.

The system consists of two levels: the feature extraction and the classification levels. The feature extraction level calculates the average grey scale and 48 texture characteristics, which are derived from the spatial grey-level co-occurrence matrices, obtained from the ROI's. The classifier level consists of three sequentially placed feed-forward Neural Networks (NN's), which are activated sequentially. The first NN classifies into normal or pathological liver regions. The pathological liver regions are classified by the second NN into cysts or "other disease". The third NN classifies "other disease" into hemangiomas and hepatocellular carcinomas. In order to enhance the performance of the classifier and improve the execution time, the dimensionality of the initial feature vector has been reduced using the sequential forward floating selection method for each individual NN input vector. A total classification rate of 98% has been achieved.

Matheus Alvarez , (2014) for a wavelet this research about Hepatocellular carcinoma (HCC) is a primary tumor of the liver. After local therapies, the tumor evaluation is based on the mRECIST criteria, which involves the measurement of the maximum diameter of the viable lesion. This paper describes a computed methodology to measure through the contrasted area of the lesions the

maximum diameter of the tumor by a computational algorithm. 63 computed tomography (CT) slices from 23 patients were assessed. Noncontrasted liver and HCC typical nodules were evaluated, and a virtual phantom was developed For this purpose.

Optimization of the algorithm detection and quantification was made using the virtual phantom. After that, We compared the algorithm findings of maximum diameter of the target lesions against radiologist measures.

Computed results of the maximum diameter are in good agreement with the results obtained by radiologist evaluation, indicating that the algorithm was able to detect properly the tumor limits. A comparison of the estimated maximum diameter by radiologist versus the algorithm revealed differences on the order of 0.25 cm for large-sized tumors (diameter > 5 cm), whereas agreement lesser than 1.0cm was found for small-sized tumors.

Differences between algorithm and radiologist measures were accurate for small-sized tumors with a trend to a small increase for tumors greater than 5 cm. Therefore, traditional methods for measuring lesion diameter should Be complemented with non-subjective measurement methods, which would allow a more correct evaluation of the contrast-enhanced areas of HCC according to the mRECIST criteria.

Another author [Herwig Wendt et al ,2012] Wrote about Image classification often relies on texture characterization. Yet texture characterization has so far rarely been based on a true 2D multifractal analysis. Recently, a 2D wavelet Leader based multifractal formalism has been proposed. It allows to perform an accurate, complete and low computational and memory costs multifractal characterization of textures in images. This contribution describes the first application of such a formalism to a real large size (publicly available) image database, consisting of 25 classes of non traditional textures, with 40 high resolution images in each class. Multifractal attributes are

estimated from each image and used as classification features within a standard k nearest neighbor classification procedure. The results reported here show that this Leader based multifractal analysis enables the effective discrimination of different textures, as performances in both classification scores and computational costs compare favorably against those of procedures previously proposed in the literature on the same database.

For daubechies wavelet [Cédric Vonesch et al , 2007] present a generalization of the orthonormal Daubechies wavelets and of their related biorthogonal flavors (Cohen-Daubechies-Feauveau, 9/7). Our fundamental constraint is that the scaling functions should reproduce a predefined set of exponential polynomials. This allows one to tune the corresponding wavelet transform to a specific class of signals, thereby ensuring good approximation and sparsity properties. The main difference with the classical construction of Daubechies et al. is that the multiresolution spaces are derived from scale-dependent generating functions. However, from an algorithmic standpoint, Mallat's Fast Wavelet Transform algorithm can still be applied; the only adaptation consists in using scale-dependent filter banks.

Finite support ensures the same computational efficiency as in the classical case. We characterize the scaling and wavelet filters, construct them and show several examples of the associated functions. We prove that these functions are square-integrable and that they converge to their classical counterparts of the corresponding order.

Another auther [Saima Rathore et al, 2011] deal with classification using Texture is a combination of repeated patterns with regular/irregular frequency. It can only be visualized but hard to describe in words. Liver structure exhibit similar behavior; it has maximum disparity in intensity texture inside and along boundary which serves as a major problem in its segmentation and classification.

Problem gets more complicated when one applies simple segmentation techniques without considering variation in intensity texture. The problem of representing liver texture is solved by encoding it in terms of certain parameters for texture analysis. Numerous textural analysis techniques have been devised for liver classification over the years some of which work equally work well for most of the imaging modalities. Here, we attempt to summarize the efficacy of textural analysis techniques devised for Computed Tomography (CT), Ultrasound and some other imaging modalities like Magnetic Resonance Imaging (MRI), in terms of well-known performance metrics.

Chapter Three

Materials and Methods

3.1 Material:

All patients examined on a Helical Multi detector CT scanner scanner (Somatom Siemens scanner dual slice, GE Dual slice, Philips Brilliance 64 slice and Aquilion ,CXXG-012A Toshiba scanner 64 slice) in Alnilein Medical Diagnostic Center, Medical Modern Center, Dar elaj specialized hospital and Royal care international hospital respectively, used for collecting data from CT Abdominal images. With 8 second rotation Time, Large SFOV, 120 kVp and (250-320 mAs) which differ through the phases.

the protocol used for Abdomen scanning triple-phase helical CT with KVp of 120 and 250 to 320 mAs, slice thickness 5mm, thin data require slice thickness of 5mm for reformatted images.

3.2 Design of the study:

This is an analytical study where selected the patient selected conventionally.

3.3 Population of the study:

The population of this study was data set (patients with CT Abdomen using triple phase portocol), The study include both gender with their age ranged from 26 years to 89 years old.

3.4 Sample size and type:

This study consisted of 180 patients diagnosed with hepatocellular carcinoma (HCC).

3.5 Data collection

Data collected from radiologist reports with Special designed sheet from findings which appear in different CT cuts. The variable data collected from the acquisition of the CT image .

3.6 Data based acquisition:

Technique : Imaging protocols :Images from 180 patients was gathered. The acquisitions were performed with MDCT device and the standardized acquisition protocol was applied: helical scanning, with lice thickness 5 mm for each patient, an appropriate amount of 60% Iodinated Contrast material (about 70 - 90 ml), was injected at 4 ml/s rate. The acquisition of the images in the arterial phase started about 20 seconds after contrast injection. Images corresponding to how the contrast acting with liver tissue (arterial , vinous and delay phase) were acquired with delay of 50–60s sequences with single Breath-holds. All images had a size of 512×512 pixels with 8-bit gray levels and were represented in DICOM format.

3.7 Methods of analysis:

The images that collected from the PACS viewed using RadiAnt Dicom Viewer software , Then the images in DICOM format were converted to JPEG image to suit IDL manipulation, Then the image were read by IDL in JEPG format and the user clicks on areas represents the back ground, HCC, normal liver, spine and ribs. The pixel intensity in these areas was assigned as classification centre, and by using the Euclidian distance between these classes and all the pixels the whole image classified into one of these classes. Then the classification map were further processed by region label to segment the liver from the rest of the structure and convert the segmented live from the classification map to binary image to extract the HCC from the whole original image.

The extracted features classified into; HCC, liver, spine and ribs. to extract the features using Gray level Run Length Matrix (GLRLM).

When using GLRLM in this study we clicks on areas represents these classes; in these areas a window of 3×3 pixel were set and the higher order statistic were calculated, which include Short Run Emphasis (SRE), Long Run Emphasis (LRE), Gray-Level Nonuniformity (GLN), Run Length Nonuniformity (RLN), Run Percentage (RP),

Low Gray-Level Run Emphasis (LGLRE), High Gray-Level Run Emphasis (HGLRE), Short Run Low Gray-Level Emphasis (SRLGLE), Short Run High Gray-Level Emphasis (SRHGLE), Long Run Low Gray-Level Emphasis (LRLGLE), Long Run High Gray-Level Emphasis (LRHGLE), These features were assigned as classification centre used by the Euclidian distances to classify the whole image. The algorithm scans the whole image using a window of 3×3 pixel and computes the higher order statistic and computes the distance (the Euclidean distance) between the calculated features and the class's centers and assigns the window to the class with the lowest distance. Then the window interlaced one pixel and the same process started over till the entire image were classified and a classification map were generated. After all images were classified the data concerning the HCC, liver, spine and ribs entered into SPSS with its classes to generate a classification score using stepwise linear discriminate analysis; to select the most discriminate features that can be used in the classification of HCC.

3.8 Ethical approval

The ethical approval was granted from the hospital and the radiology department; which include commitment of no disclose any information concerning the patient identification.

Chapter Four

4.1 Results

The main goal of this study to characterize the hepatocellular carcinoma in CT Images , the patients who diagnosed with HCC and examined by Computed Tomography , and the characterization of image done by higher order statistic and Daubechies coefficient based on Texture Analysis.

The study include 180 patients with hepatocellular carcinoma The result of this study represented in figures and tables.

Table (4.1) Shows Gender distribution of patients with HCC

Gender	***Frequency***	***Percentage***
Male	79	44 %
Female	101	56 %

Figure 4.1 show gender distribution of patients with HCC

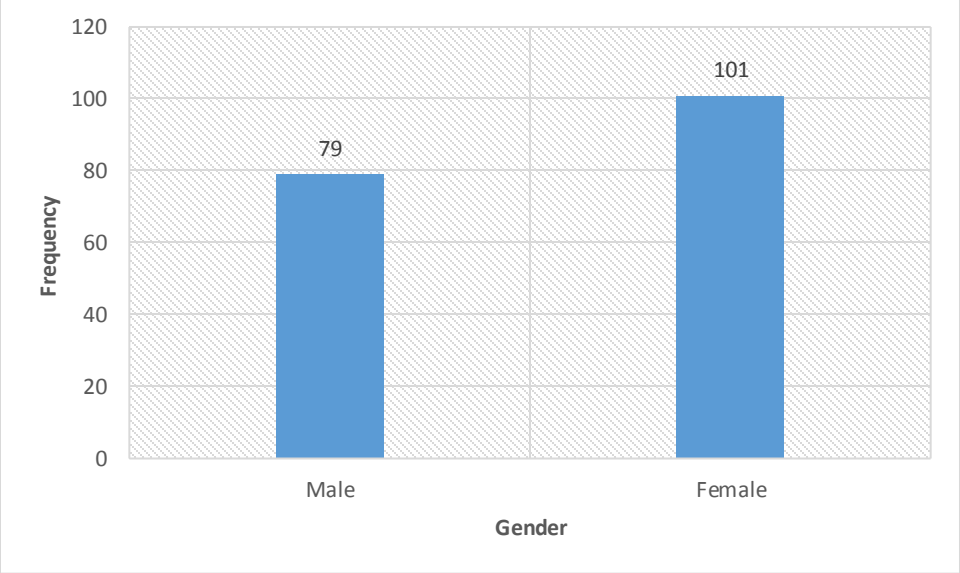

Gray Level Run Length Matrix (GLRLM):

Figure 4.2 show Scatter plot generated using discriminante analysis function for four classes represents: HCC, Liver, Spine and Ribs .

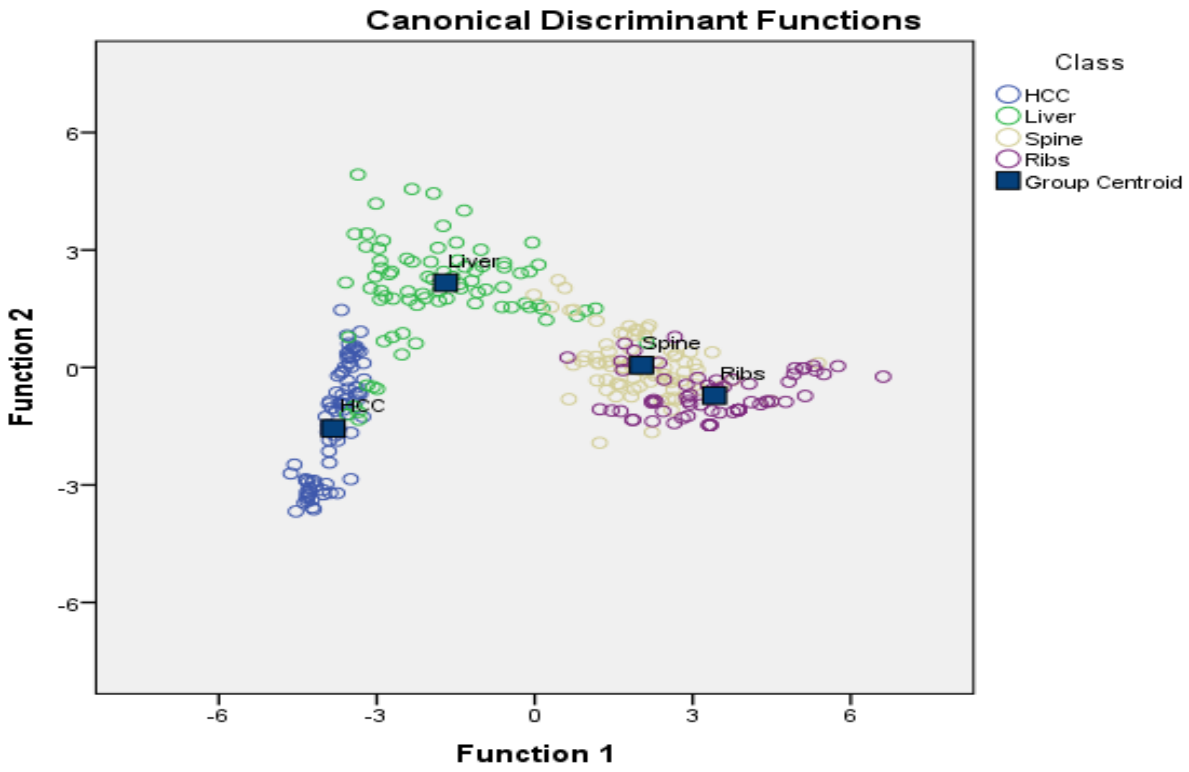

Table 4- 2 Classification score matrix generated by linear discriminate analysis with classification accuracy of 85.4%.

Original group		**Predicted Group Membership**				
		HCC	**Liver**	**Spine**	**Ribs**	**Total**
Classes	HCC	**98.8**	1.2	0	0	100%
	Liver	9.9	**85.2**	4.9	0	100%
	Spine	0	6.2	**75.3**	18.5	100%
	Ribs	0	0	18.1	**81.9**	100%
Total classification accuracy = 85.4%						

Figure 4.3show error bar plot for the Short Run Emphasis (SRE) textural features.

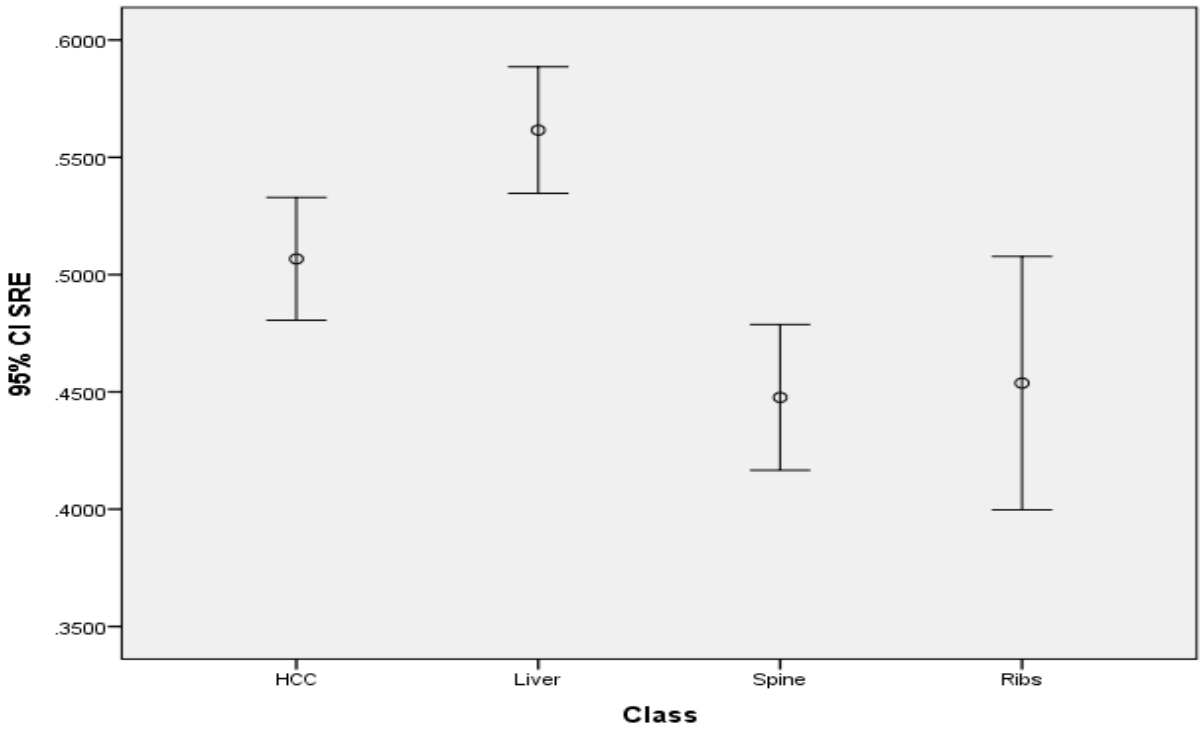

Figure 4.4 show error bar plot for the Gray Level Non-uniformity (GLN)

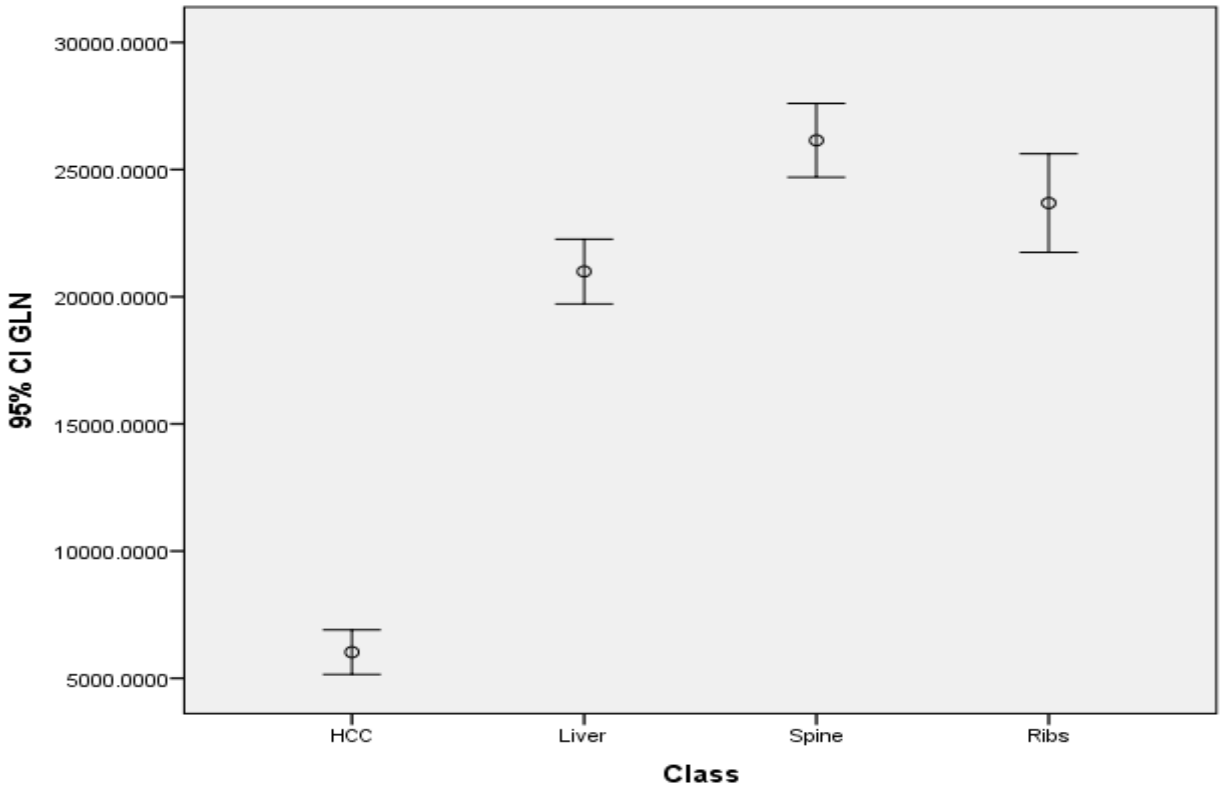

Figure 4.5 show error bar plot for the High Gray Level Run Emphasis (HGRE)

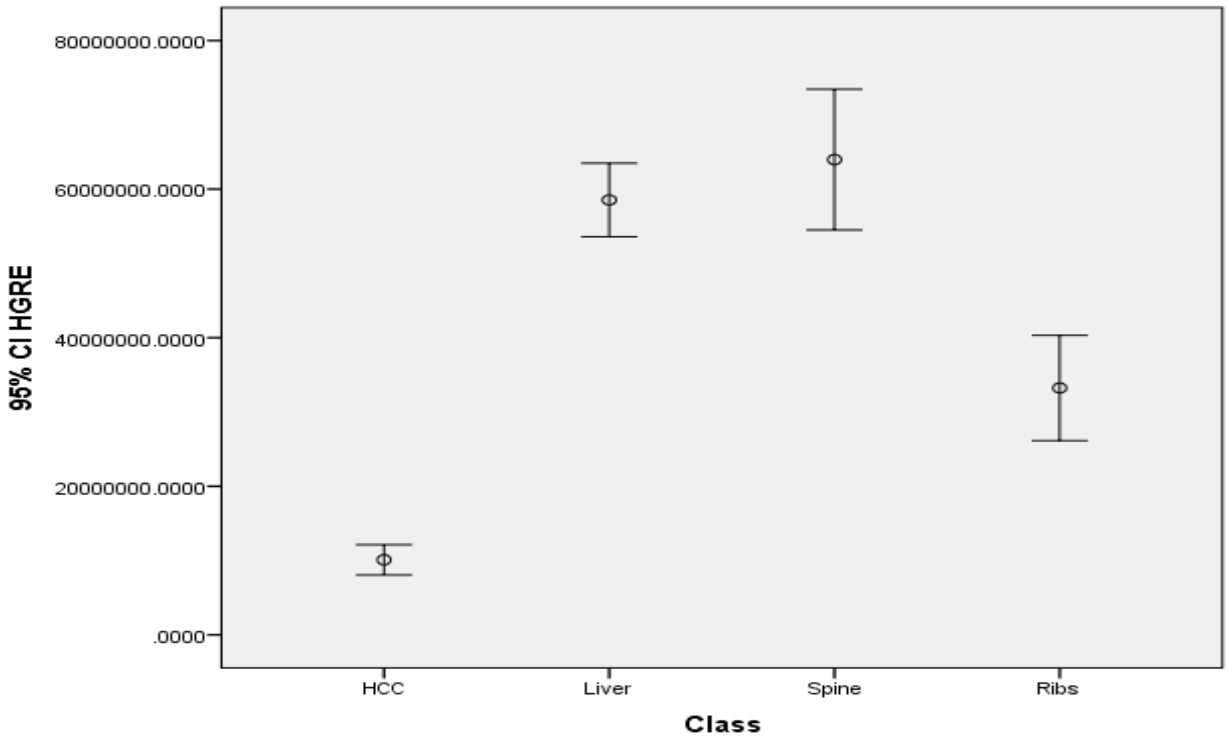

Figure 4.6 show error bar plot for the Short Run High Gray Level Emphasis (SRHGLE)

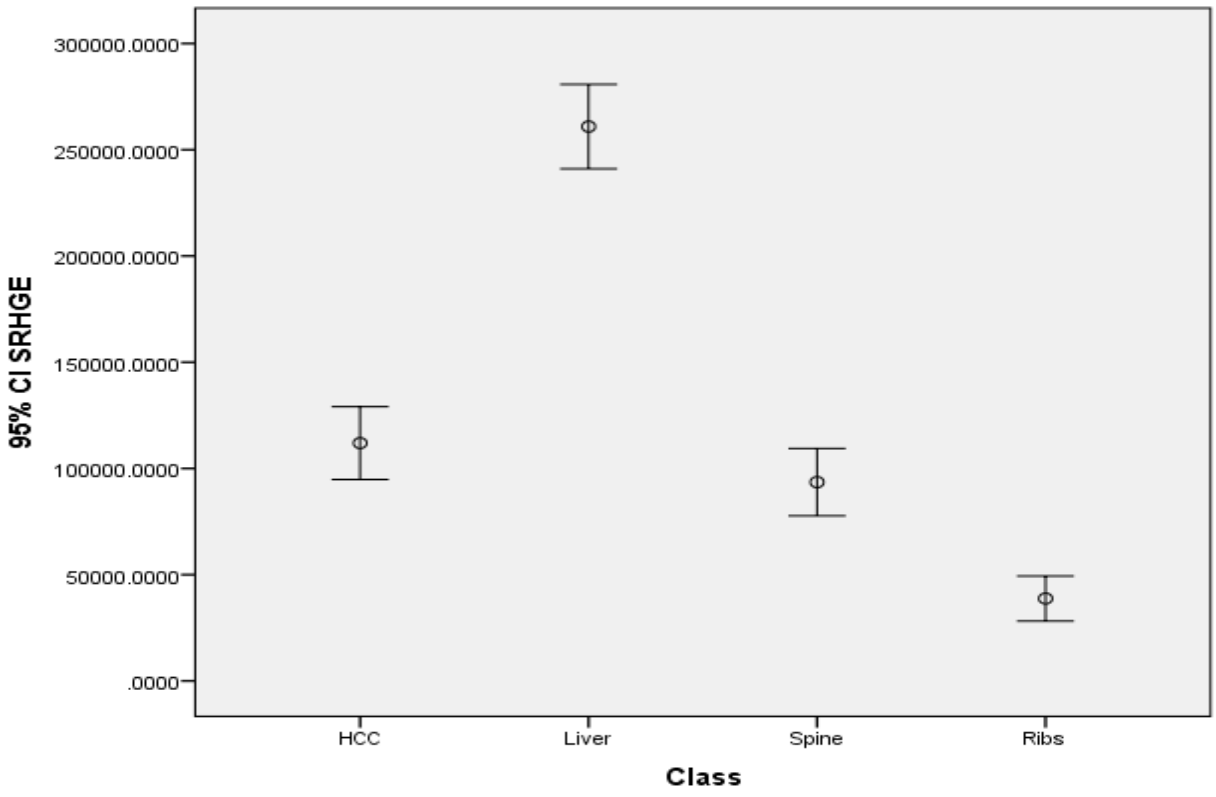

Figure 4.7 show error bar plot for the Long Run Low Gray Level Emphasis (LRLGE)

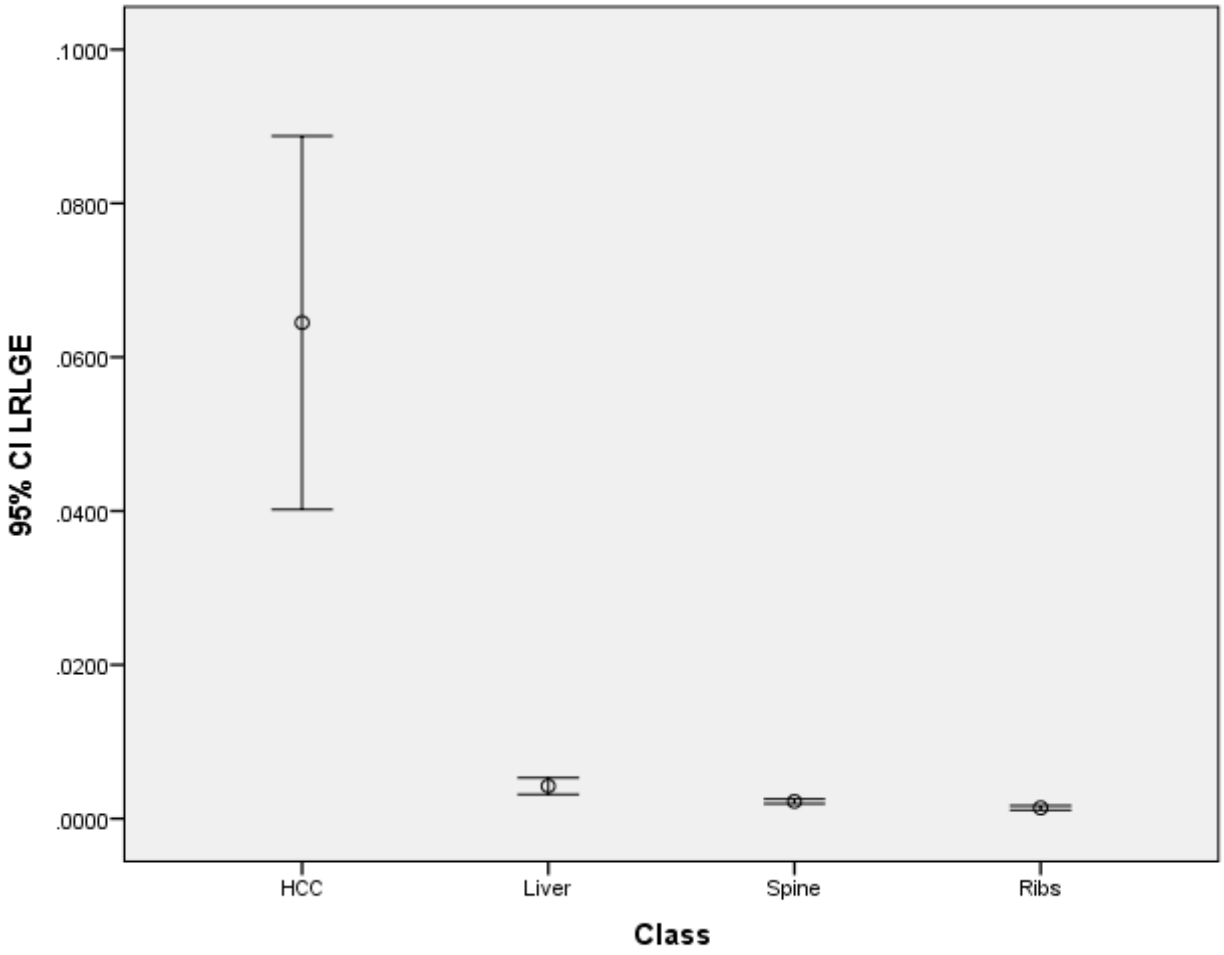
.1000
.0800
.0600
.0400
.0200
.0000
95% CI LRLGE
HCC
Liver
Spine
Ribs
Class

Daubechies wavelets based on Texture Analysis

In this section the features were extracted from Hepatocellular Carcinoma (HCC) CT images using Daubechies wavelets based on Texture Analysis. and this features showed significant correlation with the predefined classes (HCC, Liver, Spine and Ribs) .

Figure 4.8 show Scatter plot generated using discriminante analysis function for four classes represents: HCC, Liver, Spine and Ribs.

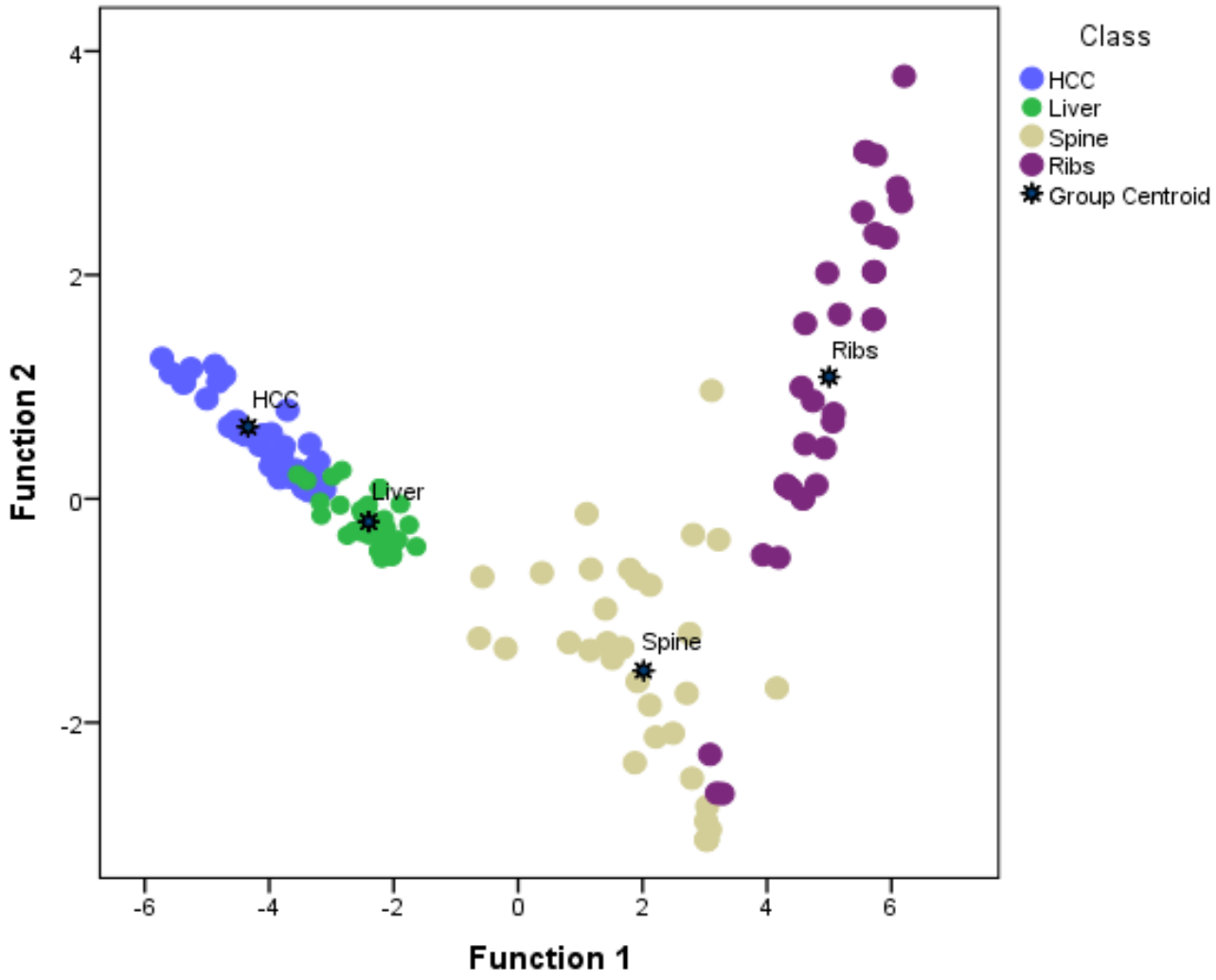

Table 4.3 Showed the classification accuracy of the HCC using linear discriminant analysis:

Classes		Predicted Group Membership				Total
		HCC	Liver	Spine	Ribs	
Original	HCC	**97.1**	2.9	.0	.0	100.0
	Liver	8.3	**91.7**	.0	.0	100.0
	Spine	2.9	.0	**97.1**	.0	100.0
	Ribs	.0	.0	8.8	**91.2**	100.0

94.2% of original grouped cases correctly classified

Figure 4.9 CT images image (A) and classification map (B), the original image (A) classified to (B) color map demonstrate the liver lesion.

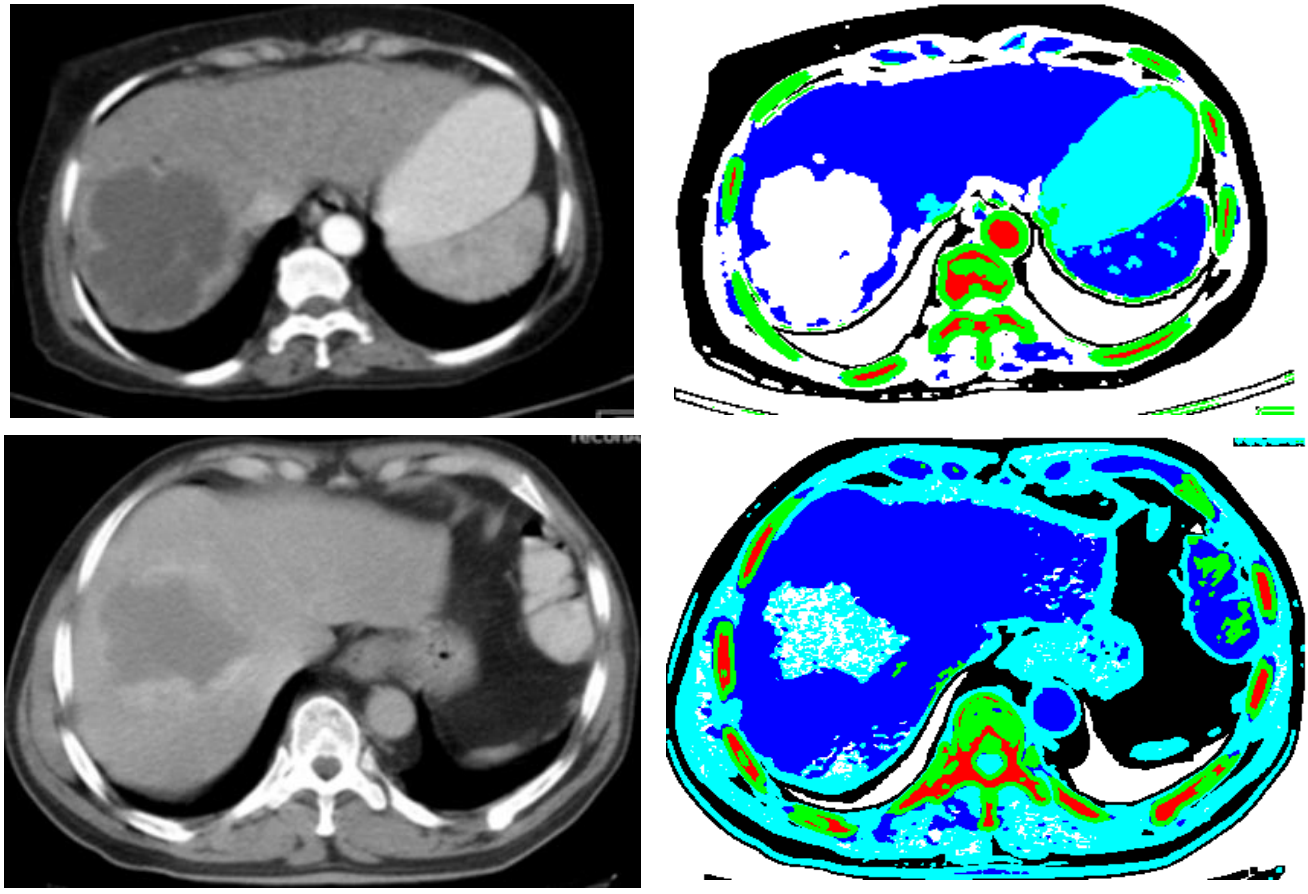

(A) ***(B)***

Chapter Five

Discussion, Conclusion and Recommendations

5.1 Discussion:

By the increasing use of direct digital imaging systems for medical diagnostics, digital image processing becomes more and more important in health care.

Digital imaging technologies have become indispensable components for clinical procedures. Major advances in the field of medical imaging and computer technology have created opportunity for quantitative analyses of medical images and provided powerful techniques to probe the structure, pathology and function of the human body. The availability of many different imaging modalities increased the requirement for significant innovations to obtain accurate and fast results in all aspect of image processing.

However, in characterization of hepatocellular carcinoma using CT images The system involves use of different measures, such as texture features (GLRLM), grey scale, fractal dimension estimators or shape descriptors, combined with a classifier using two method of analysis the data Gray Level Run Length Matrix (GLRLM) and Daubechies wavelet based on texture analysis .

In This is analytical study, performed for 180 patients, male and female who are presented for CT Abdomen to liver abdominal using multi detector helical CT Scan (MDCT). In this study the higher order statistic (GLRLM) contain elven features extracted from Triple phase CT images using 3×3 window. Three of them showed well classification with the predefined classes (HCC, Liver, Spine and Ribs) they includes short run emphasis , gray level non-uniformity , high gray level run emphasis , short run high gray level emphasis and long run low gray level emphasis .

Table 4.1 shows Gender distribution for hepatocellular carcinoma patient's, show that the female had higher rate 44:56 % male to female, and figure 4.1 show the distribution of gender where 79 represent the male and 101 represent the female.

Figure 4.2 show Scatter plot generated using discriminate analysis function for four classes represents: HCC, Liver, Spine and Ribs , with the Gray Level Run Length Matrix (GLRLM) and the classification showed that the HCC were classified well.

Table 4- 2 show Classification score matrix generated by linear discriminate analysis for the scatter plot, the linear discrimination analysis was applied to assign the classified region to their respective class, in order to find the accuracy of classification. Where the classification accuracy for the whole classes was 85.4%, with 98.8% classification for HCC, liver, spine and ribs was 85.2%, 75.3 and 81.9 respectively.

Figures 4.3 , 4.4, 4.5, 4.6 and 4.7 show Error bar plot for the Short Run Emphasis (SRE) , Error bar plot for the Gray Level Non-uniformity (GLN), Error bar plot for the High Gray Level Run Emphasis (HGRE), Error bar plot for the Short Run High Gray Level Emphasis (SRHGLE) and Error bar plot for the Long Run Low Gray Level Emphasis (LRLGE), that selected by the linear stepwise discriminate function as a discriminate feature where it discriminate between all features between HCC, Liver, Spine and Ribs . were computed from Gray Level Run Length Matrix (GLRLM) and the results are represented that there is a well concentration of features around the class centers which give a remarkable difference among the four classes especially between the HCC and liver.

Figure 4.8 show Scatter plot generated using discriminante analysis function for four classes represents: HCC, Liver, Spine and Ribs , with the Daubechies wavelet based texture analysis and the classification showed that the HCC were classified well.

Table 4-3 show Classification score matrix generated by linear discriminate analysis for the scatter plot, the linear discrimination analysis was applied to assign the classified region to their respective class, in order to find the accuracy of classification. Where the classification accuracy for the whole classes was 94.2%, with 97.1% classification for HCC, liver, spine and ribs was 91.7%, 97.1 and 91.2 respectively.

Finally, HCC and other abdominal organ in CT images for simplicity can be diagnosed and classify by using higher order statistic and Daubechies coefficient.

Excellent discrimination between hepatocellular carcinoma and other abdominal organ can be established based on GLRLM and Daubechies coefficient serves as a second method to perform more characterization of the tumor.

5.2 Conclusions :

Digital imaging technologies have become indispensable components for clinical procedures. Major advances in the field of medical imaging and computer technology have created opportunity for quantitative analyses of medical images and provided powerful techniques to probe the structure, pathology and function of the human body. The availability of many different imaging modalities increased the requirement for significant innovations to obtain accurate and fast results in all aspect of image processing.

The texture reveals a different underlying pattern of the HCC compared to the liver and other abdominal tissues with classification sensitivity 98.8%, and the combination of the GLRLM throughout the different triphasic image phases provides the highest predictive overall accuracy of 85.4 % using stepwise linear discriminant analysis.

In the Daubechies wavelet transformation the classification sensitivity 97.1 %, and the combination of the texture features throughout the different triphasic image phases provides the highest predictive overall accuracy of 94.2 % using stepwise linear discriminant analysis.

This study dictate that texture analysis is superior to visual perception system where texture reveals the change and the difference of the image pattern objectively in respect to the ground truth.

Gray level intensity values can be used as a valuable quantitative tool that would be helpful in improving the confidence in HCC diagnosis as well as facilitating more accurate diagnosis.

5.3 Recommendations

- Existing techniques can be applied to classify and differentiate other types of liver lesions.
- More texture features and techniques can be used to improve the performance.
- Texture analysis can be carried out in all image slices where the tumor were visible therefore to get volume of the tumor and this can be used for planning process of diagnostic radiotherapy treatment.
- Study can also be done in depth for other types of medical images like US and MRI .
- Initiation of image processing unit in the radiology department can help a lot in activation of image processing projects.
- Further classification of liver that associated with any hepatic disease.

References :

Ahmet Gurakar, M.D. , James P. Hamilton, Ayman Koteish, Zhiping Li, American Cancer Society. Cancer Facts & Figures 2014. Atlanta, Ga: American Cancer Society; 2014.

American Joint Committee on Cancer. Liver. In: AJCC Cancer Staging Manual. 7th ed. New York, NY: Springer; 2010:191–195

Bartlett DL, DiBisceglie AM, Dawson LA. Cancer of the liver. In: DeVita VT, Lawrence TS, Rosenberg SA, eds. DeVita, Hellman, and Rosenberg's *Cancer: Principles and Practice of Oncology*. 9th ed. Philadelphia, Pa: Lippincott Williams & Wilkins; 2011:997–1018.

Bruix J, Sherman M. Management of hepatocellular carcinoma. *Hepatology*. 2005;42:1208–1230.

Bajscy, R. (1973). Computer description of textured surfaces, Proceedings of the Joint Conference on Artificial Intelligence, August, pp. 572-579.

Conners, R. & Harlow, C. (1980). Theoretical comparison of texture algorithms. IEEE Transactions on Pattern Analysis and Machine Intelligence, Vol. 2, No. 3, pp. 204-222.

Distani, R.; Nappi, M. & Riccio, D. (2006). A range/domain approximation error-based approach for fractal image compression.IEEE Transactions on Image Processing, Vol. 15, No. 1, pp. 89-97.

El-Serag HB. Hepatocellular carcinoma. *N Engl J Med*. 2011;365:1118-1127.

Forner A, Llovet JM, Bruix J. Hepatocellular carcinoma. *Lancet*. 2012;379:1245-1255.

Esteban Mezey, M.D , Hepatocellular Carcinoma (Liver Cancer), Copyright 2001-2013 | All Rights Reserved.600 North Wolfe Street, Baltimore, Maryland 21287

Grossmann, and J. Morlet, `Decomposition of Hardy functions into square integrable wavelets of constantshape.'SIAM J. Math. Anal.,15, 723-736, (1984).

Daubechies, I.TEN LECTURES ON WAVELETS. 2nd ed. Philadelphia: SIAM, 1992. CBMS-NSF regional conference series in applied mathematics 61.

Esgiar, A.; Naguib, R.; Sharif, B.; Bennet, M. & Murray, A. (2002). Fractal analysis in the detection of colonic cancer images. IEEE Transactions on Information Technology in Biomedicine, Vol. 6, No. 1, pp 54-58.

Calderbank, A. R. and I. Daubechies , W. Sweldens, B.-L. Yeo WAVELET TRANSFORMS THAT MAP INTEGERS TO INTEGERS. Proceedings of the IEEE Conference on Image Processing. Preprint, 1996. IEEE Press, 1997. To appear.

Galloway, M.M. (1975). Texture analysis using grey-level run lengths. Computer Graphics and Image Processing, Vol. 4, pp. 172-179.

Haralick, R.M.; Shanmugam K. & Dinstein, I. Texture features for image classification.IEEE Transactions on Pattern Analysis and Machine Intelligence, Vol. SMC-3, No. 6, Nov 1973, 610-621.

ICRU, (1999). International Commission on Radiation Units and Measurements. ICRU Report 62: Prescribing, Recording and Reporting Photon Beam Therapy (Supplement to ICRU 50), Oxford University Press.

Bruno A., Collorec R., Bézy-Wendling J., Reuzé P., Rolland Y.: Texture analysis in medical imaging, In: Roux C., Coatrieux J. L. (Eds.): Contemporary Perspectives in Three-dimensional Biomedical Imaging, IOS Press 1997, 133–164.

Haralick R. M.: Statistical and structural approaches to texture, Proc. IEEE 1979, 67, 786–804.

Haralick R. M., Shanmugam K., Dinstein I.: Textural features for image classification. IEEE Trans- actions on Systems, Man and Cybernetics 1973, 3, 610–621.

Galloway M. M.: Texture analysis using gray level run lengths. Computer Graphics and Image Pro- cessing 1975, 4, 172–179.

Chen C., Daponte J. S., Fox M. D.: Fractal feature analysis and classification in medical imaging, IEEE Transactions on Medical Imaging 1989, 8, 133–142.

Cross G. R., Jain A. K.: Markov random fields texture models. IEEE Transactions on Pattern Analysis and Machine Intelligence 1985, 5(1), 25–39.

Clausi D. A., Jernigan M. E.: Designing gabor filters for optimal texture separability. Pattern Reco- gnition 2000, 33, 1836–1849.

Mallat S. G.: A theory for multiresolution signal decomposition: The wavelet representation. IEEE Transactions on Pattern Analysis and Machine Intelligence 1989, 11(7), 674–693.

Haralick R., Sternberg S. R., Zhuang X.: Image analysis using mathematical morphology. IEEE Transactions on Pattern Analysis and Machine Intelligence 1989, 9(4), 532–550.

Herlidou-Meme S., Constans J. M., Carsin B., Olivié D., Eliat P. A., Nadal-Desbarats L., Gondry C., Le Rumeur E., Idy-Peretti I., de Certaines J.D.: MRI texture analysis on texture test objects, normal brain and intracranial tumors. Magnetic Resonance Imaging 2003, 21, 989–993.

Joo S., Yang Y. S., Moon W. K., Kim H. C.: Computer-aided diagnosis of solid breast nodules: use of an artificial neural network based on multiple sonographic features. IEEE Transactions on Medical Imaging 2004, 23(10), 1292–1300.

Chappard D., Chennebault A., Moreau M., Legrand E., Audran, M., Basle M. F.: Texture analysis of X-ray radiograms is a more reliable descriptor of bone loss than mineral content in a rat model of localized disuse induced by the Clostridium botulinum toxin. Bone 2001, 28(1), 72–79.

dos Santos Filho E., Yoshizawa M., Tanaka, A., Saijo, Y., Yambe T., Nitta, S.: Toward a neuro-fuzzy system for automatic segmentation and characterization of intravascular ultrasound images. SICE Annual Conference 2003, 2, 1586–1589.

Gletsos M., Mougiakakou S. G., Matsopoulos G. K., Nikita K. S., Nikita A. S., Kelekis D.: A computer-aided diagnostic system to characterize CT focal liver lesions: design and optimization of

a Neural Network classifier, IEEE Transactions on Information Technology in Biomedicine 2003, 7(3), 153–162.

Mir A. H., Hanmandlu M., Tandon S. N.: Texture analysis of CT-images, IEEE Engineering in Me- dicine and Biology 1995, 5, 781–786.

Chen E. L., Chung P. C., Chen C. L., Tsai H. M., Chang C. I.: An automatic diagnostic system for CT liver image classification. IEEE Transactions on Biomedical Engineering 1998, 45(6), 783–794.

Husain S. A., Shigeru E.: Use of neutral networks for feature based recognition of liver region on CT images, Proc. of the IEEE Signal Processing Society Workshop 2000, 2, 831–840.

Sariyanni C. P. A., Asvestas P., Matsopoulos G. K., Nikita K. S., Nikita A. S. Kelekis D.: A fractal analysis of CT liver images for the discrimination of hepatic lesions: A comparative study, Proc. of the 23rd Annual EMBS International Conference 2001, 1557–1560.

J. Morlet, G. Arens, I. Fourgeau, and D. Giard, `Wave Propagation and Sampling Theory.', Geophysics., 47, 203-236, (1982).

Julesz, B. (1975). Experiments in the visual perception of texture. Scientific American, Vol. 232, pp 34-43.

Kachouie, N. & Fieguth, P. (2007). A medical texture local binary pattern for TRUS prostate segmentation, Proceedings of the 29th International Conference of the IEEE Engineering and Biology Society, Lyon, France, August 23rd– 26th.

Karahaliou, A.; Boniatis, I; Skiadopoulos, S. & Sakellaropoulos, F. (2008). Breast cancer diagnosis: analyzing texture of tissue surrounding microcalcifications. IEEE Transactions on Information Technology in Biomedicine, Vol. 12, No. 6, pp. 731-738.

Kovalev, V.; Kruggel, F.; Gertz, H. & von Cramon D. (2001). Three-dimensional texture analysis of MRI brain datasets. IEEE Transactions on Medical Imaging, Vol. 20, No. 5, pp. 424-433.

Krętowski M., Bezy-Wendling J., Duda D.: Classification of hepatic metastasis in enhanced CT nimages by dipolar decision tree, Proc. of 19th GRETSI 2003, 327–330.

Duda D., Krętowski M., Bézy-Wendling J.: Texture-based classification of hepatic primary tumors in multiphase CT. Proc. of 7th MICCAI, LNCS Springer-Verlag 2004, 3217, 1050–1051.

Kurani, A.; Xu, D.; Furst, J. & Raicu, D. (2004). Co-occurrence matrices for volumetric data, Proceedings of 7th IASTED International Conference on Computer Graphics and Imaging, Kauai, Hawaii, USA, August 17 th – 19th

Mettler, F.A., Jr.,Medical Radiation Exposure in the U.S. in 2006: Preliminary Results. *Health Physics* **95**, 502-507 510.1097/1001.HP.332 (2008).

T.M. Deserno (ed.),Biomedical Image Processing, Biological and Medical Physics,Biomedical Engineering, DOI: 10.1007/978-3-642-15816-21,

.Mirmehdi, M.; Xie, X. & Suri, J. (eds) (2008). Handbook of texture analysis, Imperial College Press, 1-84816-115-8, UK.

Nailon, W.H. & Ironside, J.W. (2000) Variant Creutzfeldt-Jakob disease: immunocytochemical studies and image analysis. Microscopy Research & Technique, Vol. 50, No. 1, pp. 2-9.

Pietikainen, M.K. (ed) (2000). Texture analysis in machine vision, World Scientific Publishing, 981-02-4373-1, Singapore.

Press, W.; Flannery, B.; Teulkolsky, S. & Vetterling, W. Numerical recipes in C: the art of scientific computing. Cambridge University Press, ISBN 0-521-35465-X, UK.

Tuceryan, M. & Jain, A.K. (1998). Texture analysis. In: Chen, C.H; Pau, L.F. & Wang, P.S.P., (eds). The handbook of pattern recognition and computer vision. 22 nded. World Scientific Publishing Co., ISBN 9-810-23071-0, Singapore .

Sheng, Y. WAVELET TRANSFORM. In: The transforms and applications handbook. Ed. by A. D. Poularikas. P. 747-827. Boca Raton, Fl (USA): CRC Press, 1996. The Electrical Engineering Handbook Series.

Uppaluri, R.; Mitsa, T.; Sonka, M.; Hoffman, E. & McLennan G. (1997). Quantification of pulmonary emphysema from lung computed tomography images. American Journal of Respiratory Care in Medicine, Vol. 156, No. 1, pp. 248-254.

Weber, A.G. (2004). The USC texture mosaics.University of Southern California Viterbi School of Engineering, http://sipi.usc.edu/ .

Valavanis I., Mougiakakou S. G., Nikita K. S., Nikita A.: Computer aided diagnosis of CT focal liver lesions by an ensemble of neural network and statistical classifiers, Proc. of the IEEE International Joint Conference on Neural Networks 2004, 3, 1929–1934.

World Gastroenterology Organisation, 2009 .

Winzenrieth, R. & Claude, I. (2006). Is there functional vascular information in anatomical MR sequences? A preliminary in vivo study. IEEE Transactions on Biomedical Engineering, Vol. 53, No. 6, June 2006, pp.1190-1194.

Xu, Y.; Sonka, G.; McLennan, G.; Junfeng, G. & Hoffman, E. (2006). CT-based 3D texture classification of emphysema and early smoking related pathologies. IEEE Transactions on Medical Imaging, Vol. 25, No. 4, pp. 464-475.

Y. Hoshida, A. Villanueva, M. Kobayashi et al., Gene expression in fixed tissues and outcome in hepatocellular carcinoma, N Engl J Med 359(19) (6 Nov 2008), 1995–2004.

Zhou, B.; Xuan, J.; Zhao, H.; Chepko, M.; Freedman, M. & Yingyin, K. (2007). Polarization imaging for breast cancer diagnosis using texture analysis and svm, Proceedings of Life Sciences Systems and Applications Workshop, pp. 217-220, Bethesda, Maryland, USA.